Hadronic deformation energy. I. Quark-antiquark separation*

Carleton DeTar†

Center for Theoretical Physics, Laboratory for Nuclear Science and Department of Physics, Massachusetts Institute of Technology, Cambridge, Massachusetts 02139

(Received 1 July 1977)

The MIT bag model for hadrons is treated in the static cavity approximation in three dimensions with a definite quark number. The energy of the system is computed to second order in the gluon coupling. A constrained variational method is described which permits the calculation of the energy as a function of a collective variable. The bag cavity is permitted to assume whatever shape of a general class is necessary in order to minimize the energy for a given expectation value of the collective variable. The method is well suited for the study of the two-nucleon interaction at short range. By way of introducing the computational procedure the method is here applied to a bag containing one quark and one antiquark and the energy as a function of a measure of the separation of the quarks is evaluated.

I. INTRODUCTION

The MIT bag model of hadrons[1] in the static cavity approximation accounts remarkably well for the static properties of the light hadrons[2] (the octets of pseudoscalar and vector mesons and the lowest baryon octet and decuplet). The construction of the model is appealing simple.[3] Its ingredients are the currently fashionable combination of quarks of three colors and three or four flavors and an octet of colored vector gluons, confined to a finite volume by a uniform pressure, the key innovation of the model. Nonstrange quarks are massless, the hadronic mass scale being set by the confining pressure.

Calculations of the static properties of hadrons composed of the light quarks have, to date, made use of a spherical cavity, since the noninteracting fermion and gluon eigenfunctions are known for this geometry. Moreover it was expected that any deviations from a spherical shape required to balance the field pressure against the uniform confining pressure would not alter the results significantly. Rebbi[4] has studeid the effects of small fluctuations from spherical shapes. Hasenfratz, Kuti, and Szalay[5] have reported calculations for a deformed static cavity containing a massive-charmed-quark-antiquark pair treated as classical point sources of the gluon electric fields. They obtain the spin-independent part of an effective potential for charmonium which exhibits a linear increase at large quark separation.

The present investigation of deformations of the hadrons has been motivated by an interest in understanding properties of the interactions of hadrons composed of the light quarks. The first step in this direction involves studying adiabatic deformations of the cavity in which the light degrees of freedom—quarks and gluons—adjust instantaneously to the changing cavity shape. Such an approach should be applicable to the study of hadronic interactions which involve low velocities for the hadrons. In particular the two-nucleon interaction near threshold seems particularly well suited to this approach.

By way of introducing the computational techniques to be used in the study of interaction of the two-nucleon system we present here results of an investigation of the simpler problem of the deformation energy of a hadron composed of a light quark and antiquark as a function of their separation. In particular we consider cavity shapes with axial symmetry and a reflection symmetry in the equatorial plane and restrict our attention to the state corresponding to the ρ meson with spin projection $|m_s| = 1$ on the axis of deformation. The results are in agreement with what is expected from other arguments[5,6] and provide support for the reliability of the computational method. The application to the two-nucleon problem is left to the following paper.[7]

In the static cavity approximation[2] the quark fields are expressed in terms of the fermion creation and annihilation operators for the cavity eigenmodes

$$q(\vec{x},t)=\sum_n [\, q_n(\vec{x})e^{-i\omega_n t}b_n + \tilde{q}_n(\vec{x})e^{i\omega_n t}d_n^\dagger \,] , \quad (1.1)$$

where q_n satisfies the Dirac equation for energy ω_n inside the cavity

$$(-i\vec{\alpha}\cdot\nabla+\beta m)q_n(\vec{x})=\omega_n q_n(\vec{x}) , \quad (1.2)$$

with $\tilde{q}_n$ the corresponding antiparticle wave function. The linear boundary condition on the surface of the cavity

$$i\vec{\alpha}\cdot\hat{n}q_n(\vec{x})=-\gamma_0 q_n(\vec{x}) , \quad (1.3)$$

where $\hat{n}$ is the unit outward normal to the surface

ensures that the baryonic current does not penetrate the surface, i.e., $\hat{n}\cdot q_n^\dagger \vec{\alpha} q_m = 0$ on the surface. The quark wave functions are normalized so that

$$\int q_n^\dagger q_m \, dV = \delta_{nm}\,, \qquad \int q_n^\dagger \tilde{q}_m \, dV = 0\,. \tag{1.4}$$

They must also satisfy a quadratic boundary condition which is discussed below.

We describe in Sec. II approximations leading to an effective Hamiltonian to second order in the gluon coupling for a cavity containing only quarks. It is of the form

$$H = \int \{ :q^\dagger(-i\alpha\cdot\nabla + \beta m)q: + \tfrac{1}{2}[(\vec{E}^a)^2 + (\vec{B}^a)^2] - \vec{J}^a\cdot\vec{A}^a + B\}\, dV + E_0(V)\,. \tag{1.5}$$

The effective Hamiltonian is constructed so that its expectation value on a cavity state gives the cavity energy to second order in the gluon coupling. The gluons behave like Maxwell fields to this order and are produced by the fermion color current:

$$j_\mu^a = g :\bar{q}\lambda^a \gamma_\mu q:\,. \tag{1.6}$$

In the static limit they satisfy

$$\nabla\cdot\vec{E}^a = j^{0a}\,, \quad \nabla\times\vec{B}^a = \vec{J}^a \text{ in } V\,, \tag{1.7}$$

$$\hat{n}\cdot\vec{E}^a = 0\,, \quad \hat{n}\times\vec{B}^a = 0 \text{ on } S\,. \tag{1.8}$$

In the usual notation, g is the gluon coupling constant, λ^a are the 3×3 matrix generators of color SU(3) normalized so that $(\lambda^a)^2 = \frac{16}{3}$. (Summation over the color index a is always understood.) Because of the linear boundary condition on $\vec{E}^a$, only color-singlet states can exist. The constant B is the term which provides the confining pressure and is renormalized by the zero-point energy of the fields.[2] The finite part of the gluon and fermion zero-point energy is given by E_0, which depends on the shape of the cavity. The fermion energy term is accordingly normal-ordered. The order of magnitude of $E_0(V)$ is known from studies of the light hadrons, and its effect can be estimated qualitatively as discussed in Sec. III E.

The shape of the cavity in the absence of external constraints is determined by requiring that the expectation value of the Hamiltonian be minimized with respect to variations in its shape. This procedure results in imposing a nonlinear surface boundary condition on the fields, which can be interpreted as balancing the field pressure against B; but for computational purposes it is more useful to impose this boundary condition variationally. Thus for a given cavity state and energy

$$|\psi(V)\rangle \text{ and } E(V) = \langle\psi(V)|H|\psi(V)\rangle\,,$$

the conditions

$$\frac{\delta}{\delta V}E(V) = 0\,, \quad \frac{\delta^2}{\delta V^2}E(V) > 0 \tag{1.9}$$

determine the shape of the hadron.[8]

In general the conditions (1.9) require knowing the cavity energy for arbitrary shapes for which one faces the difficult task of solving the Dirac and Maxwell equations in a cavity of arbitrary shape subject to the various linear boundary conditions—a task which is impossible analytically. Even elliptically shaped cavities pose what are probably insurmountable problems for the fermion eigenstates.[9] Various numerical and approximate techniques are available, however. One could set up a coordinate mesh and solve the equations numerically. A variational approach was taken instead, since it was readily adaptable to the problem of fixing a chosen collective variable. Trail fermion wave functions q_n and trial gluon vector potentials A_μ^a are constructed for the ground state. For a given fixed shape the parameters characterizing q_n and A_μ^a are varied and the stationary point

$$\frac{\delta}{\delta q_n}\langle H\rangle = 0\,, \quad \frac{\delta}{\delta A_\mu}\langle H\rangle = 0 \tag{1.10}$$

is located. Actually the precise form of the effective Hamiltonian (1.5) cannot be used for this procedure because it is not positive definite, but if some care is taken, the stationary point of the proper variational expression provides an approximation to the solution of the Dirac and Maxwell equations and the linear boundary conditions. The method is discussed in Sec. III.

Thus the problem can be regarded as being entirely variational with respect to the parameters characterizing the cavity shape and wave functions. To find the energy as a function of the expectation value of an operator $\mathcal{O}$,

$$\bar{\mathcal{O}} = \langle\psi(V)|\,\mathcal{O}\,|\psi(V)\rangle\,, \tag{1.11}$$

one simply adds the usual Lagrange constraint to the Hamiltonian,

$$H \to H - c_{\mathcal{O}}\mathcal{O}, \tag{1.12}$$

and from the stationary point, obtains $E(c_{\mathcal{O}})$ and $\bar{\mathcal{O}}(c_{\mathcal{O}})$.

When the constrained Hamiltonian (1.12) is minimized, the equations of motion and the boundary conditions are altered by the constraint. Since the new form of the equations of motion and boundary conditions can be rather complex, depending on the nature of the constraint, the variational approach is a convenient vehicle for the formulation of the constraint.

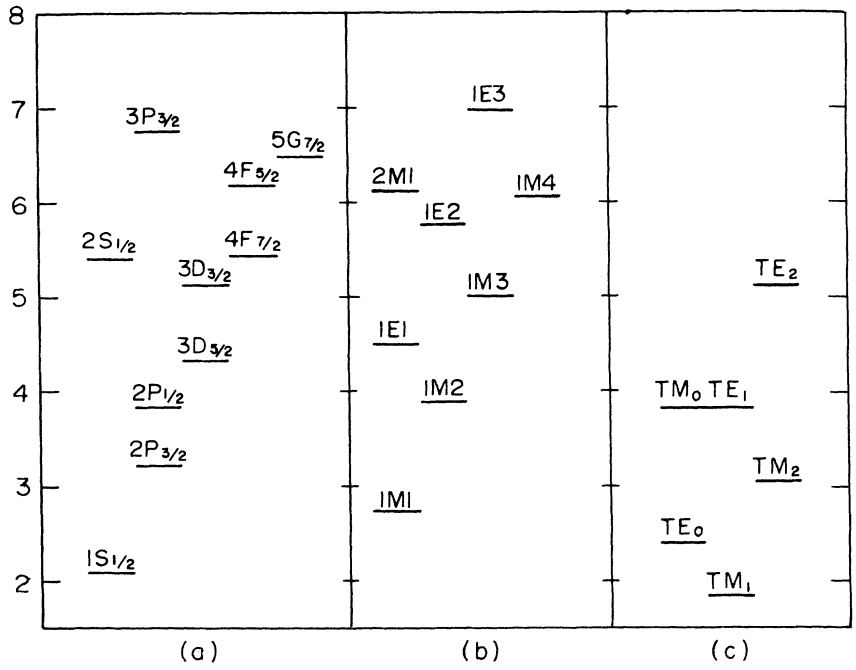

FIG. 1. (a) Lowest eigenenergies (units of $B^{1/4}$) for massless fermions in a unit sphere (i.e., of radius $1\times B^{-1/4}$ in terms of the bag constant B). The spectroscopic notation refers to the angular momentum content of the upper two components of the Dirac spinor [A. Chodos and C. B. Thorn, Nucl. Phys. B104, 21 (1976)]. (b) Lowest eigenenergies (units of $B^{1/4}$) for gluons in a unit sphere. The notations nMj and nEj refer to the radial (n) and total angular momentum (j) quantum numbers for magnetic and electric multipoles. (c) Lowest eigenenergies (units of $B^{1/4}$) for gluons in an infinite cylinder of unit radius. The notations TM_m and TE_m refer to the absolute value (m) of the magnetic quantum number for the transverse-magnetic and transverse-electric modes. (Only the lowest radial mode appears in each case.) The correspondence between gluon levels for cylinder and sphere is shown in Table I.

The remainder of the paper is organized as follows. In Sec. II we describe the orbital configuration of the quarks and construct the effective second-order Hamiltonian for the cavity state containing no free gluons. In Sec. III the mechanics of the variational computation are discussed, treating the variational procedure for computing the fermion and gluon energies, the handling of the zero-point and self-energies of the fields, and finally the method of assembling the component calculations as one variational scheme. In Sec. IV the results of the computation are presented and discussed.

II. THE EFFECTIVE HAMILTONIAN

In the present calculation the separation of the quarks is achieved by constraining the orbitals to separate into a left orbital and right orbital while preserving the spatial symmetry of quark occupation, which is present in the undistorted configurations of the low-lying mesons. Thus the spatial part of the wave function is

$$q(1,2) = q_L(1)\bar{q}_R(2) + q_R(1)\bar{q}_L(2). \tag{2.1}$$

Let the deformation axis be the z axis. Expressing the left and right orbitals in terms of orthogonal orbitals symmetric and antisymmetric in $z \to -z$, we have (apart from normalization factors)

$$q_L = q_S - \sqrt{\mu}\, q_A, \quad q_R = q_S + \sqrt{\mu}\, q_A,$$
$$q(1,2) = q_S(1)\bar{q}_S(2) - \mu\, q_A(1)\bar{q}_A(2). \tag{2.2}$$

Thus we are led to consider a mixture of two orbital configurations S^2 and A^2 with the mixing parameter μ ranging from 0 to 1 for maximal to minimal overlap between the associated left and right orbitals. The mixing parameter μ is to be determined variationally by minimizing the constrained Hamiltonian.

It is convenient to use the "free" cavity eigenmodes as a basis for the description of the fermion wave functions (i.e., the eigenmodes in the absence of gluon interactions). The symmetric and antisymmetric states in (2.2) are therefore to be identified with the lowest-energy free cavity eigenmodes of the same type. For the sphere [see Fig. 1(a)], these are, respectively, the $1S_{1/2}$ and $2P_{3/2}$ orbitals in the usual nonrelativistic terminology

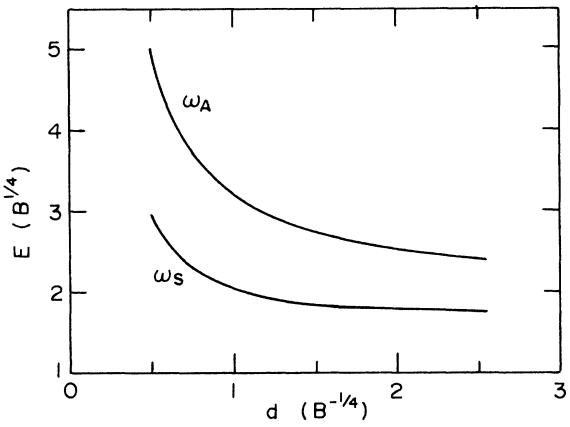

FIG. 2. Lowest fermion eigenenergies determined variationally for ellipsoidal cavity shapes with unit equatorial radius, plotted as a function of the polar radius d. For the sphere, $d=1$. (Units are given in terms of the bag constant B.)

for the upper components of the Dirac spinors. The fermion kinetic energy for the state (2.2) in the absence of gluon interactions is then given by

$$E_F = 2\frac{\omega_S + \mu^2\omega_A}{1+\mu^2}, \tag{2.3}$$

where ω_S and ω_A are the eigenenergies for the lowest symmetric and antisymmetric orbitals.

If we want to calculate the lowest-order shift in the fermion energy due to gluon interactions, we must work to second order in the interaction Hamiltonian

$$\int j^{\mu a} A^a_\mu dV, \tag{2.4}$$

since we are considering only states with quarks present. To the extent that the lowest gluon eigenenergies ω_G are considerably higher than the energy difference $\omega_S - \omega_A$ between the antisymmetric and symmetric orbitals, we may regard these orbitals as essentially degenerate in computing the second-order level shift.[10]

To what extent is the approximation justified? In Fig. 2 we show a plot of the free cavity eigenenergies ω_A and ω_S for cavities of a range of ellipsoidal shapes. (In the process of fission $\omega_A - \omega_S$ goes rapidly to zero.) Although we have not computed the gluon eigenfrequencies directly, the values for the sphere are shown in Fig. 1(b), and the values for the cylinder are shown in Fig. 1(c). The correspondence between spherical and cylindrical eigenmodes produced by an adiabatic deformation may be guessed by comparing the field configurations, and is shown in Table I. It is apparent that $(\omega_A - \omega_S)/\omega_G$ for the lowest gluon mode is of the order of $\frac{1}{3}$ or less. Improvements to this approximation would need at least to include explicitly the $q\bar{q}G$ state (state with one extra gluon) in the diagonalization of the Hamiltonian. Of course, although the second-order shift is computed as though $\omega_A \approx \omega_S$, we do not intend to ignore the level separation in treating the unperturbed fermion energy (2.3), since this difference associates an increased kinetic energy with a localization of the quarks—an effect which cannot be disregarded. Therefore our use of degenerate second-order perturbation theory requires the diagonalization of the Hamiltonian matrix

TABLE I. Correspondence of some of the lowest gluon eigenmodes of the sphere and the cylinder produced by an adiabatic deformation, as suggested by a comparison of the field configurations and spectra. The index p is the longitudinal quantum number in the notation of Jackson (Ref. 14).

	TM modes			TE modes	
m	$p=1$	$p=2$	m	$p=0$	$p=1$
0	$E_{1,0}$	$E_{2,0}$	0	$M_{1,0}$	$M_{2,0}$
1	$M_{1,\pm1}$	$M_{2,\pm1}$	1	$E_{1,\pm1}$	
2	$M_{2,\pm2}$		2	$M_{3,\pm2}$	

$$H_{\alpha\beta} = \langle\alpha|H_0|\beta\rangle + \Delta H_{\alpha\beta}, \tag{2.5a}$$

$$\Delta H_{\alpha\beta} = \sum_n \frac{\langle\alpha|\int j^{\mu a} A^a_\mu dV|n\rangle\langle n|\int j^{\mu a} A^a_\mu dV|\beta\rangle}{\omega_\alpha - \omega_n}, \tag{2.5b}$$

where H_0 is the diagonal free-quark Hamiltonian, α and β refer to the configurations SS and AA, and the intermediate state n contains one gluon. Only in computing $\Delta H_{\alpha\beta}$ is the approximation $\omega_\alpha = \omega_\beta$ used.

Let us now express the Hamiltonian (2.5) in terms of the quark creation and annihilation operators. With only two cavity eigenmodes present, the expression for the field operator for a given cavity is effectively

$$q(\vec{x}) = \sum_{c,f,m} [q_{Scfm}(\vec{x})b_{Scfm}e^{-i\omega_S t} + \bar{q}_{Scfm}(\vec{x})d^\dagger_{Scfm}e^{i\omega_S t} + q_{Acfm}(\vec{x})b_{Acfm}e^{-i\omega_A t} + \bar{q}_{Acfm}(\vec{x})d^\dagger_{Acfm}e^{i\omega_A t}], \tag{2.6}$$

where the indices c, f, and m refer to color, flavor, and spin. The c-number Dirac spinors satisfy (1.2) and (1.3) for zero quark mass. Suppressing the internal-symmetry indices now, the effective color current operator may be written schematically as

$$j^{a\mu} = j^{\mu}_{SS}(b^{\dagger}_S \lambda^a b_S - d^{\dagger}_S \lambda^a d_S) + j^{\mu}_{AA}(b^{\dagger}_A \lambda^a b_A - d^{\dagger}_A \lambda^a d_A) + j^{\mu}_{SA}(b^{\dagger}_A \lambda^a b_S + b^{\dagger}_S \lambda^a b_A - d^{\dagger}_A \lambda^a d_S - d^{\dagger}_S \lambda^a d_A), \tag{2.7}$$

where the c-number currents are given by

$$j^{\mu}_{UV} = g \bar{q}_U \gamma^{\mu} q_V. \tag{2.8}$$

Let us consider the explicit dependence on internal-symmetry quantum numbers. The spin dependence can be displayed by using the Pauli-spinor basis. For example, the contribution to the charge density and current density in the first term of (2.7) may be written as

$$[\rho^a]_{SS} = \sum_{c,c',f,m,m'} g \rho_{SS} b^{\dagger}_{Sc'fm'} \lambda^a_{c'c} \delta_{m'm} b_{Scfm}, \tag{2.9}$$

$$[\vec{J}^a]_{SS} = \sum_{i,c,c',f,m,m'} g \vec{J}_{SSi} b^{\dagger}_{Sc'fm'} \lambda^a_{c'c} \sigma^i_{m'm} b_{Scfm}.$$

The other terms have similar expansions. The c-number coefficients depend only on the cavity geometry, all of the configuration dependence having been absorbed in the bilinear combination of fermion operators.

We now consider the second-order shift in the Hamiltonian (2.5b). Since the currents are taken to be static, the sum over intermediate states reproduces the static cavity gluon propagator. Using the identities

$$\int_V (\vec{B}^a)^2 dV = \int_V \vec{J}^a \cdot \vec{A}^a dV, \tag{2.10a}$$

$$\int_V (\vec{E}^a)^2 dV = \int_V \rho^a \phi^a dV, \tag{2.10b}$$

which follow from (1.7) and (1.8) we may recast (2.5b) into the form

$$\Delta H_{\alpha\beta} = \langle \alpha | \int [\tfrac{1}{2}(\vec{B}^a)^2 + \tfrac{1}{2}(\vec{E}^a)^2 - \vec{J}^a \cdot \vec{A}^a] dV | \beta \rangle, \tag{2.11}$$

where, $\vec{A}^a$, $\vec{B}^a$, and $\vec{E}^a$ are operators bilinear in the quark creation and annihilation operators, satisfying Maxwell's equations for the operator current (2.6). The ground-state energy may then be found variationally by minimizing the expectation value of the effective Hamiltonian (1.5) on the state

$$(1+\mu^2)^{-1/2}(b^{\dagger}_S d^{\dagger}_S - \mu b^{\dagger}_A d^{\dagger}_A)|0\rangle \tag{2.12}$$

with respect to variations in μ. [In (2.12) it is understood that the internal-symmetry indices are combined so as to construct a color-singlet state with the desired total spin and isospin.]

The expectation value of the gluon terms in the effective Hamiltonian are depicted graphically in Fig. 3. It is useful to observe that the effective Hamiltonian may be expressed as a sum of terms which contain configuration-dependent operators and c-number, configuration-independent energies. For example, the unperturbed quark energy contribution is

$$\omega_S(b^{\dagger}_S b_S + d^{\dagger}_S d_S) + \omega_A(b^{\dagger}_A b_A + d^{\dagger}_A d_A), \tag{2.13}$$

where ω_S and ω_A depend only on the cavity shape. The same is true for the gluon energies, as we now demonstrate. The contribution to the electric and magnetic field operators produced by the term (2.8) may be written in the same form as the term itself, namely,

$$\begin{aligned} [\vec{E}^a]_{SS} &= \vec{E}_{SS} b^{\dagger}_S \lambda^a b_S, \\ [\vec{B}^a]_{SS} &= \sum_{i=1}^{3} \vec{B}_{SSi} b^{\dagger}_S \lambda^a \sigma^i b_S, \end{aligned} \tag{2.14}$$

where internal-symmetry labels have been suppressed. Again, the c-number coefficients $\vec{E}_{SS}$ and $\vec{B}_{SSi}$ are configuration independent and result from solving (1.7) and (1.8) for the c-number coefficients ρ_{SSi} and $\vec{J}_{SSi}$.[11] Because of the symmetry of the cavity with respect to rotations about its axis, the integration over the azimuthal angle ϕ in (2.11) results in a slight simplification for the spin-dependent terms in that only two degrees of freedom occur corresponding to spin flip and nonflip. Thus the term in the effective Hamiltonian depicted in Fig. 3(a), which results from substituting (2.14) into (2.11) and using (2.10a), has the form

$$\begin{aligned} [\vec{H}]_{SSSS} = 2(&W_{ES} b^{\dagger}_S \lambda^a b_S d^{\dagger}_S \lambda^a d_S \\ &+ W_{MSz} b^{\dagger}_S \lambda^a \sigma^3 b_S d^{\dagger}_S \lambda^a \sigma^3 d_S \\ &+ W_{MS\perp} b^{\dagger}_S \lambda^a \vec{\sigma}^{\perp} b_S d^{\dagger}_S \lambda^a \vec{\sigma}^{\perp} d_S), \end{aligned} \tag{2.15}$$

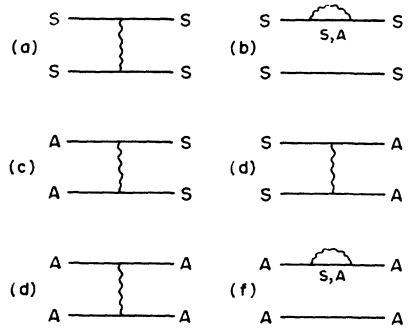

FIG. 3. Diagrams for the gluon coupling to second order in perturbation theory.

where[11]

$$W_{ES}=\tfrac{1}{2}\int \vec{E}_{SS}\cdot\vec{E}_{SS}dV,$$

$$W_{MSz}=-\tfrac{1}{2}\int \vec{B}_{SS3}\cdot\vec{B}_{SS3}dV,$$

$$W_{MS\perp}=-\tfrac{1}{2}\int \vec{B}_{SS\perp}\cdot\vec{B}_{SS\perp}dV, \qquad (2.16)$$

$$\vec{\sigma}^{\perp}=\hat{e}_1\sigma^1+\hat{e}_2\sigma^2,$$

$$\vec{B}_{SS\perp}\cdot\vec{B}_{SS\perp}=\vec{B}_{SS1}\cdot\vec{B}_{SS1}+\vec{B}_{SS2}\cdot\vec{B}_{SS2}.$$

Similarly, the remaining configuration-independent factors are as follows:

$$W_{EA}=\tfrac{1}{2}\int \vec{E}_{AA}\cdot\vec{E}_{AA}dV,$$

$$W_{MAz}=-\tfrac{1}{2}\int \vec{B}_{AA3}\cdot\vec{B}_{AA3}dV,$$

$$W_{MA\perp}=-\tfrac{1}{2}\int \vec{B}_{AA\perp}\cdot\vec{B}_{AA\perp}dV,$$

$$W_{EX}=\tfrac{1}{2}\int \vec{E}_{AS}\cdot\vec{E}_{SA}dV,$$

$$W_{EXz}=\tfrac{1}{2}\int \vec{E}_{AS3}\cdot\vec{E}_{SA3}dV, \qquad (2.17)$$

$$W_{EX\perp}=\tfrac{1}{2}\int \vec{E}_{AS\perp}\cdot\vec{E}_{SA\perp}dV,$$

$$W_{MX}=-\tfrac{1}{2}\int \vec{B}_{AS}\cdot\vec{B}_{SA}dV,$$

$$W_{MXz}=-\tfrac{1}{2}\int \vec{B}_{AS3}\cdot\vec{B}_{SA3}dV,$$

$$W_{MX\perp}=-\tfrac{1}{2}\int \vec{B}_{AS\perp}\cdot\vec{B}_{SA\perp}dV.$$

The expectation value of the effective Hamiltonian on the state (2.12) may now be written

$$\begin{aligned}E=&n_S\omega_S+n_A\omega_A+(W_{MSz}C_{Sz}+W_{MS\perp}C_{S\perp})\\&+(W_{MAz}+W_{MA\perp}C_{A\perp})+(W_{MX\perp}-W_{EX\perp})C_{X\perp}\\&+(W_{MXz}+W_{EXz})C_{Xz}+(W_{EX}+W_{MX})C_X\\&+E_{self}+E_0+BV,\end{aligned} \qquad (2.17a)$$

where the contribution to the self-energy from the S and A orbitals is

$$\begin{aligned}E_{self}=&n^c_{Sz}W_{MSz}+n^c_{S\perp}W_{MS\perp}+n^c_{Az}W_{MAz}\\&+n^c_{A\perp}W_{MA\perp}+(n^c_S+n^c_A)W_{EX}\\&+(n^c_{Sz}+n^c_{Az})(W_{MXz}+W_{EXz})\\&+(n^c_{S\perp}+n^c_{A\perp})(W_{MX\perp}-W_{EX\perp}).\end{aligned} \qquad (2.17b)$$

The configuration-dependent coefficients in (2.17) are

$$\begin{aligned}&n_S=\langle b^\dagger_S b_S+d^\dagger_S d_S\rangle,\quad n_A=\langle b^\dagger_A b_A+d^\dagger_A d_A\rangle,\\&C_{Sz}=2\langle b^\dagger_S\sigma^3\lambda^a b_S d^\dagger_S\sigma^3\lambda^a d_S\rangle,\\&C_{S\perp}=2\langle b^\dagger_S\vec{\sigma}^{\perp}\lambda^a b_S d^\dagger_S\vec{\sigma}^{\perp}\lambda^a d_S\rangle,\\&C_{Az}=2\langle b^\dagger_A\sigma^3\lambda^a b_A d^\dagger_A\sigma^3\lambda^a d_A\rangle,\\&C_{A\perp}=2\langle b^\dagger_A\vec{\sigma}^{\perp}\lambda^a b_A d^\dagger_A\vec{\sigma}^{\perp}\lambda^a d_A\rangle,\\&C_{Xz}=2\langle b^\dagger_A\sigma^3\lambda^a b_S d^\dagger_A\sigma^3\lambda^a d_S+(S\rightleftharpoons A)\rangle,\\&C_{X\perp}=2\langle b^\dagger_A\vec{\sigma}^{\perp}\lambda^a b_S d^\dagger_A\vec{\sigma}^{\perp}\lambda^a d_S+(S\rightleftharpoons A)\rangle,\\&C_X=2\langle b^\dagger_A\lambda^a b_S d^\dagger_A\lambda^a d_S+(S\rightleftharpoons A)\rangle,\\&n^c_S=\langle b^\dagger_S(\lambda^a)^2 b_S+d^\dagger_S(\lambda^a)^2 d_S\rangle,\\&n^c_A=\langle b^\dagger_A(\lambda^a)^2 b_A+d^\dagger_A(\lambda^a)^2 d_A\rangle,\\&n^c_{Sz}=\langle b^\dagger_S(\lambda^a\sigma^3)^2 b_S+d^\dagger_S(\lambda^a\sigma^3)^2 d_S\rangle,\\&n^c_{Az}=\langle b^\dagger_A(\lambda^a\sigma^3)^2 b_A+d^\dagger_A(\lambda^a\sigma^3)^2 d_A\rangle,\\&n^c_{S\perp}=\langle b^\dagger_S(\lambda^a\vec{\sigma}^{\perp})^2 b_S+d^\dagger_S(\lambda^a\vec{\sigma}^{\perp})^2 d_S\rangle,\\&n^c_{A\perp}=\langle b^\dagger_A(\lambda^a\vec{\sigma}^{\perp})^2 b_A+d^\dagger_A(\lambda^a\vec{\sigma}^{\perp})^2 d_A\rangle.\end{aligned} \qquad (2.18)$$

The terms in (2.17) and (2.18) with subscript X correspond to the exchange graphs in Figs. 3(c) and 3(d). The first two terms in parentheses in (2.17a) correspond to the graphs in Figs. 3(a) and 3(e), respectively. Details concerning the contributions of the exchange graphs, the self-energy E_{self}, and zero-point energy E_0 are given in Secs. III E and III F. In writing (2.17) we have made use of the property[2] that the operators

$$b^\dagger_S\lambda^a b_S+d^\dagger_S\lambda^a d_S \text{ and } b^\dagger_A\lambda^a b_A+d^\dagger_A\lambda^a d_A \qquad (2.19)$$

annihilate the quark-antiquark color singlet state (2.12). *A fortiori*

$$\langle b^\dagger_S\lambda^a b_S b^\dagger_S\lambda^a b_S\rangle+\langle d^\dagger_S\lambda^a d_S d^\dagger_S\lambda^a d_S\rangle+2\langle b^\dagger_S\lambda^a b_S d^\dagger_S\lambda^a d_S\rangle=0, \qquad (2.20)$$

and similarly for the antisymmetric orbital. Thus the electric part of the self-energy graphs S-S-S and A-A-A in Figs. 3(b) and 3(f) cancel the color-electric contributions from the gluon-exchange graphs Figs. 3(a) and 3(e), and the terms W_{AS} and W_{ES} do not enter in (2.17).

Finally we write the values of the configuration-dependent operators on the state (2.12) corresponding to a ρ meson with spin projection $|m_S|=1$ on the deformation axis:

$$\begin{aligned}&n_s=2/N,\quad n_A=2-n_S,\quad N=1+\mu^2,\\&C_{Sz}=2/N(-\tfrac{16}{3}),\quad C_{Az}=\mu^2 C_{Sz},\\&C_{Xz}=4\mu/N(-\tfrac{16}{3}),\quad C_X=4\mu/N(\tfrac{16}{3}),\\&C_{S\perp}=C_{A\perp}=C_{X\perp}=0,\\&n^c_{Sz}=\tfrac{1}{2}n^c_{S\perp}=n^c_S=\tfrac{16}{3}n_S,\\&n^c_{Az}=\tfrac{1}{2}n^c_{A\perp}=n^c_A=\tfrac{16}{3}n_A.\end{aligned} \qquad (2.21)$$

The expressions for other spins and isospins are also easily obtained.

III. THE VARIATIONAL APPROACH TO THE QUARK AND GLUON ENERGIES

In this section we discuss the way the variational principle is put into practice by considering the component parts of the computation in the order in which the calculation was carried out. The effect of combining them is discussed in subsection G of this section.

A. The bag geometry

In the present study a three-parameter azimuthally symmetric surface has been considered, defined in cylindrical coordinates by

$$\rho^2=\rho_S{}^2(z)=n^2(1-z^2/d^2)(1+az^2/d^2)\,, \tag{3.1}$$

where n is the cylindrical radius at $z=0$, d is the length of extension in z, and

$$\begin{aligned}
&a=0 \ \text{ellipse}\,,\\
&-1<a<0 \ \text{distorted ellipse—bulge in middle}\,,\\
&0<a<1 \ \text{distorted ellipse—flattened in middle}\,,\\
&1<a \ \text{peanut shape}\,,\\
&a\to\infty\,,\ n\to 0 \ \text{fission}\,,\\
&-\infty<a<-1 \ \text{two bags}\,.
\end{aligned} \tag{3.2}$$

A considerable variety of shapes can be studied with such a parametrization, although it has a distinct limitation in that at the point of fission the two bag components have a teardrop configuration. This leads to a ~10% overestimate of the two-bag energy at this point which could be remedied by adding terms cubic in z^2 and higher.

B. Unperturbed fermion wave function

The variational approach to finding the ground-state wave function for the Dirac equation is complicated by the fact that the Hamiltonian is not positive definite or negative definite. Thus we have chosen to minimize the expectation value of the square of the Dirac Hamiltonian

$$\omega_n{}^2=\int q_n^\dagger(i\alpha\cdot\vec{\nabla}+\beta m)(-i\alpha\cdot\vec{\nabla}+\beta m)q_n\,dV\Big/\int q_n^\dagger q_n\,dV\,. \tag{3.3}$$

Since the linear boundary condition is not reproduced by an unconstrained variation of this expression with respect to q, it is imposed explicitly in the construction of the trial expression for q:

$$i\vec{\alpha}\cdot\hat{n}\,q_n(\vec{x})=-\gamma^0 q_n(\vec{x}) \text{ on } S\,. \tag{3.4}$$

Variation of ω^2 with q so constrained leads to the boundary condition

$$\vec{\alpha}\cdot\hat{n}(-i\alpha\cdot\nabla+\beta m)q_n=-\gamma^0(-i\alpha\cdot\nabla+\beta m)q_n\,, \tag{3.5}$$

which is compatible with (3.4) when q_n satisfies the Dirac equation.[12]

Although minimization of (3.3) leads to an upper bound on the true value of the square of the ground-state energy, it does not determine the eigenfunction uniquely, since particle and antiparticle wave functions give the same value for ω^2. Thus given any trial function q_0 which minimizes ω^2, there is a one-parameter family

$$q_\lambda=\exp(\tfrac{1}{2}\lambda\gamma_0\gamma_5)q_0=(\cos\tfrac{1}{2}\lambda)q_0+(\sin\tfrac{1}{2}\lambda)\gamma_0\gamma_5 q_0\,, \tag{3.6}$$

which has the same value of ω^2. To select the function which most nearly represents a state of positive energy, it suffices to maximize

$$\omega_\lambda=\int q_\lambda^\dagger(-i\alpha\cdot\vec{\nabla}+\beta m)q_\lambda\,dV\Big/\int q^\dagger q\,dV \tag{3.7}$$

with respect to λ. Our choice of trial function has the feature that it maximizes ω_λ automatically, so this step is unnecessary.

The trial functions are constructed with the aid of the vector $\vec{s}$ and contour function $R^2(\rho,z)$ defined as follows:

$$\begin{aligned}
&R^2(\rho,z)=R_0{}^2+\rho^2-\rho_s{}^2(z)\,,\\
&R_0{}^2=\max_z\,\rho_s{}^2(z)\,,\\
&\vec{s}=\nabla R/\nu\,,\quad \nu=\left|\nabla R\right|_{\rho=\rho_s(z)}\,.
\end{aligned} \tag{3.8}$$

Because (3.1) defines the surface, $R^2(\rho,z)=R_0{}^2$ also defines the surface. Thus the gradient of R defines the surface normal and $\vec{s}$ is the unit normal to the surface. For the sphere of radius $R_0=n=d$, $R^2=r^2$ and $\vec{s}=\vec{r}/R_0$. If $\rho_s{}^2$ were sufficiently general, we would have for a cylinder $R^2=\rho^2$ and $\vec{s}=\vec{\rho}/R_0$ and for two equal spheres, $\vec{s}=\vec{r}_1/R_0$ and $\vec{r}_2/R_0$ for the respective spherical radius vectors.

The trial expressions for the fermion spinors are constructed in terms of four scalar wave functions ϕ_A, ϕ_S, χ_A, and χ_S as follows:

$$q_{Sm}=\begin{pmatrix}\phi_S\,U_m\\ i\vec{\sigma}\cdot\vec{s}\chi_S U_m\end{pmatrix}\,, \tag{3.9a}$$

$$q_{Am}=\begin{pmatrix}\phi_A z U_m\\ i\vec{\sigma}\cdot\vec{s}\chi_A z U_m\end{pmatrix}-\kappa\begin{pmatrix}\vec{\sigma}\cdot\vec{s}\sigma_z\phi_A U_m\\ is^2\sigma_z\chi_A U_m\end{pmatrix}\,, \tag{3.9b}$$

where

$$\begin{aligned}
&\phi_S=\beta_S+\alpha_S[\rho^2-\rho_s{}^2(z)]\,,\\
&\chi_S=\beta_S+\gamma_S[\rho^2-\rho_s{}^2(z)]\,,\\
&\phi_A=\beta_A+\alpha_A[\rho^2-\rho_s{}^2(z)]\,,\\
&\chi_A=\beta_A+\gamma_A[\rho^2-\rho_s{}^2(z)]\,,
\end{aligned} \tag{3.10}$$

and U_m is a two-component Pauli spinor. Only the $m=\pm\frac{1}{2}$ states are considered so that $U_m=\binom{1}{0}$ or $\binom{0}{1}$. The constant κ is fixed by requiring that q_{Am} be orthogonal to the trial antiparticle version of q_{Sm} (a state of the same parity). Thus

$$\int q^{\dagger}_{Am'} q_{Sm}\, dV = 0\,, \tag{3.11}$$

where

$$q_{Sm}=\begin{pmatrix} \vec{\sigma}\cdot\hat{s}\sigma_z \chi_S U_m \\ \sigma_z i\phi_S U_m \end{pmatrix}\,. \tag{3.12}$$

Since, by construction, $\phi_S=\chi_S$ and $\phi_A=\chi_A$ on the surface, the trial functions satisfy the linear boundary condition (1.3) explicitly.

It is interesting to compare the trial expressions with the exact expressions known for the unit sphere (i.e., a sphere of radius $1\times B^{-1/4}$). Apart from overall normalization factors, the replacements

$$\begin{aligned} &\phi_S=j_0(\omega_S r)\,,\quad \chi_S=j_1(\omega_S r)/r\,,\\ &\phi_A=j_1(\omega_A r)/r\,,\quad \chi_A=j_2(\omega_A r)/r^2\,,\quad \kappa=\tfrac{1}{3}\,, \end{aligned} \tag{3.13}$$

where the j_n are spherical Bessel functions, yield the exact solution. Thus the trial expressions for the sphere amount to a polynomial approximation to the low-order spherical Bessel functions. In Fig. 4 we present a comparison of the exact and variationally determined wave functions ϕ_S, ϕ_A, χ_S, and χ_A for the sphere. The agreement is excellent. The eigenenergies so determined in units of $B^{1/4}$,

$$\begin{aligned} &\omega_S=2.045\,,\\ &\omega_A=3.214\,, \end{aligned} \tag{3.14}$$

differ by a fraction of one percent from the known exact values ($\omega_S=2.043$, $\omega_A=3.204$). It is necessary to take care in constructing the quark wave functions since errors in these wave functions propagate into the determination of the gluon energies where errors of a few percent are encountered.

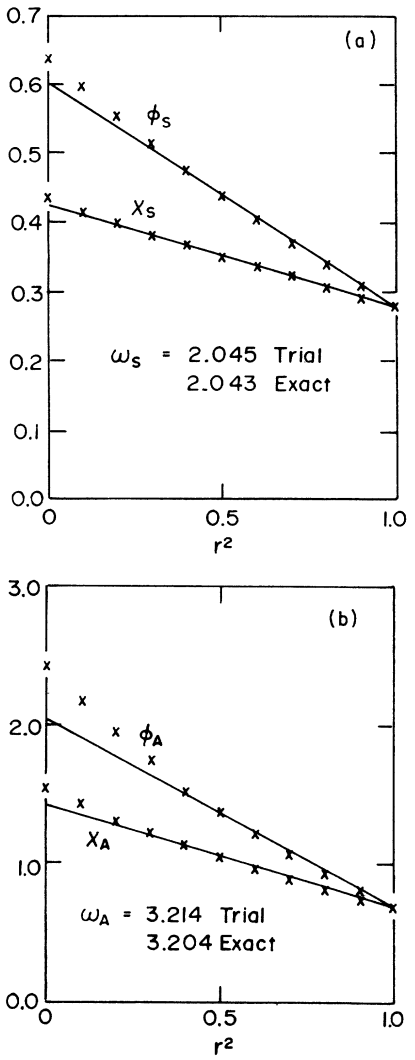

FIG. 4. Comparison of normalized exact and best trial eigenfunctions defining the $1S_{1/2}$ (a) and $2P_{3/2}$ (b) fermion orbitals for the unit sphere. The solid lines give the trial value based on the expressions (3.10) and the crosses show the exact values based on (3.13).

C. Gluon fields

In the approximation of Sec. II the gluon fields are to be calculated as though the currents derived from the free cavity fermion orbitals were static. Of course the diagonal currents (i.e., those not involving a change of orbital) are exactly static. However, for the transition current it was helpful to construct solutions to the time-dependent Maxwell equations since the solutions can then be compared with exact ones available for the sphere; moreover, with the time dependence taken into account, the currents are conserved, to the extent that the fermion wave functions satisfy the Dirac equation. This procedure, in any case, does not affect the accuracy of the results any more than the original approximation of degeneracy, since the gluon energies are altered by the *square* of the ratio of the current frequency to the lowest gluon frequency, or about 10% at worst. (Taking the time dependence into account here does not restore any precision lost in making the approximation of degenerate perturbation theory in Sec. II; the proper way to do so involves including explicitly in the calculation states with gluons.)

The gluon fields and energies are found by a variational procedure described below for the

static color magnetic, static color electric, and transition fields.

1. Static color-magnetic field

The expression

$$W_M = \tfrac{1}{2}\int \vec{B}\cdot\vec{B}dV - \int \vec{J}\cdot\vec{A}dV \tag{3.15}$$

with $\vec{B} = \nabla\times\vec{A}$ is a minimum with respect to variations in $\vec{A}$ when

$$\nabla\times\vec{B} = \vec{J} \text{ in } V, \qquad \hat{n}\times\vec{B} = 0 \text{ on } S\,. \tag{3.16}$$

Thus both the equation of motion and the linear boundary condition arise from a variation principle. The linear boundary condition arises from permitting $\vec{A}$ to vary without restriction on the surface when seeking the minimum. If the current is conserved and $\hat{n}\cdot\vec{J} = 0$ on the surface, then a gauge transformation on $\vec{A}$ produces no change in W_M. Since the currents in the present application are to be constructed from trial solutions to the Dirac equation, they are not exactly conserved. This property can cause problems with the variational calculation, since an appropriate gauge transformation can make W_M arbitrarily negative. To remedy this problem the gauge may be fixed variationally. It is convenient to use the gauge

$$\vec{s}\circ\vec{A} = 0\,, \tag{3.17}$$

where $\vec{s}$ is defined in (3.8). The modified variational expression

$$W_M = \int [\tfrac{1}{2}\vec{B}^2 - \vec{J}\cdot\vec{A} + \tfrac{1}{2}(\vec{A}\cdot\vec{s})^2]\,dV \tag{3.18}$$

is bounded below. Minimizing the above expression yields the equations

$$\vec{A}\cdot\vec{s} \equiv \vec{A}\cdot\hat{n} = 0\,,\quad \hat{n}\times\vec{B} = 0 \text{ on } S\,, \qquad \nabla\times\vec{B} = \vec{J} - \vec{s}(\vec{A}\cdot\vec{s}) \text{ in } V\,. \tag{3.19}$$

Thus the nonconserved part of $\vec{J}$ determines $A\cdot\vec{s}$ through

$$\nabla\cdot\vec{J} = \nabla\cdot[\vec{s}(\vec{A}\cdot\vec{s})] \text{ in } V\,. \tag{3.20}$$

At the minimum

$$W_M = -\tfrac{1}{2}\int \vec{B}^2 dV - \tfrac{1}{2}\int (\vec{A}\cdot\vec{s})^2 dV\,. \tag{3.21}$$

The latter term must be removed from W_M to obtain a correct estimate of the energy. When the current is conserved it vanishes. Since the currents are nearly conserved in the present calculation, its contribution is quite small. In practice, therefore, the gauge has simply been fixed *explicitly* in the construction of the trial vector potentials in accordance with (3.17).

The currents for the S-S and A-A diagonal transition based on the trial spinors (3.9) take the form

$$\begin{aligned}\vec{J}_{SS} &= 2g\phi_S\,\chi_S\vec{\sigma}\times\vec{s}\\ \vec{J}_{AA} &= 2g\phi_A\,\chi_A[\vec{J}\times\vec{s}(z^2 - 2\kappa z s_z)\\ &\quad + (\vec{\sigma}\times\vec{s} - 2\sigma_z\hat{z}\times\vec{s})\kappa^2 s^2 + 2\vec{\sigma}\cdot\vec{s}\hat{z}\times\vec{s}\kappa z]\,.\end{aligned} \tag{3.22}$$

In the notation of (2.9)

$$(\vec{J}_{SS})_{mm'} = \sum_i \vec{J}_{SSi}\,\sigma^i_{mm'}\,. \tag{3.23}$$

For the unit sphere $\vec{s}\to\vec{r}$ and $\kappa\to\frac{1}{3}$ and, as expected, the currents have the angular momentum content appropriate for exciting magnetic dipole and octupole gluon terms,

$$\begin{aligned}\vec{J}_{SS} &= \vec{r}\times\nabla[\,j_{1S}(\sigma\cdot\vec{r})]\,,\\ \vec{J}_{AA} &= \vec{r}\times\nabla[\,j_{SA}(\vec{\sigma}\cdot\vec{r}z^2 - \tfrac{2}{5}z\sigma_z r^2 - \tfrac{1}{5}\vec{\sigma}\cdot\vec{r}r^2)\\ &\quad + j_{1A}(\sigma_z z - 2\vec{\sigma}\cdot\vec{r})]\,,\end{aligned} \tag{3.24}$$

where

$$j_{1S} = -2g\phi_S\chi_S\,,\quad j_{1A} = \tfrac{8}{45}\,\phi_A\chi_A r^2\,,\quad j_{3A} = -\tfrac{2}{3}g\phi_A\chi_A \tag{3.25}$$

are the two dipole and octupole coefficients, respectively.

The corresponding vector potentials were chosen to imitate the form of the current. For the sphere and cylinder this procedure is appropriate for finding the exact soution. Thus

$$\vec{A}_{SS} = a_S\vec{\sigma}\times\vec{s}\,, \tag{3.26}$$

$$\vec{A}_{AA} = a_A\vec{\sigma}\times\vec{s} + d_A z^2\vec{\sigma}\times\vec{s} + b_A z\,\vec{s}\times\hat{z}\vec{\sigma}\cdot\vec{s} + c_A\hat{z}\times\vec{s}\sigma_z\,,$$

where the scalar functions a_A, a_S, b_A, c_A, and d_A are simple polynomials in R^2 (3.8).

As a check of this parameterization, the variationally determined coefficients for the vector potentials based on the trial fermion currents are compared in the Appendix, Table II, and Fig. 5 with the exact solutions known for the unit sphere. The agreement is quite satisfactory and shows that the contributions to the energies are determined correctly to within a couple percent.

2. Static electric field

In the state (2.12) under consideration the fermions never appear in both the S and A orbitals simultaneously. Hence the relation (2.20) holds and the static electric fields produced by the diagonal currents S-S and A-A in the gluon-exchange diagrams are completely canceled by the self-energy contributions. However, when more general orbital configurations occur in which fermions appear simultaneously in different orbitals, there is a

net contribution. We discuss it here for the sake of completeness.

The expression

$$W_B = -\tfrac{1}{2}\int \mathbf{E}^2 dV + \int \rho\phi\, dV\,, \tag{3.27}$$

with $\vec{\mathbf{E}} = -\nabla\phi$ is *maximized* with respect to variations in ϕ when

$$\nabla\cdot\vec{\mathbf{E}} = \rho \text{ in } V\,,\quad \hat{n}\cdot\vec{\mathbf{E}} = 0 \text{ on } S\,. \tag{3.28}$$

The surface boundary condition is obtained when variations of ϕ on the surface are unrestricted. No problems with gauge dependence and incompatibility with the boundary condition arise since the charge densities ρ to be considered all have the property that the condition

$$\int \rho\, dV = 0 \tag{3.29}$$

is met exactly.

Because the effective Hamiltonian is evaluated on a color singlet state, only the difference between the diagonal charge densities in the two orbitals ever appears, and likewise only the difference between the fields which they produce.

With the trial parameterization (3.9a), the difference in charge densities is

$$\begin{aligned}\rho_D &= \rho_{SS} - \rho_{AA}\\ &= g[\phi_S{}^2 + \chi_s{}^2 s^2\\ &\quad -(\phi_A{}^2 + s^2\chi_A{}^2)(z^2 + s^2\kappa^2 - 2zs_z\kappa)]\,.\end{aligned} \tag{3.30}$$

For the sphere $s^2 \to r^2, s_z \to z$, $\kappa \to \frac{1}{3}$, electric mono-

TABLE II. A comparison of exact and trial energies for the massless quarks and for various components of the color magnetic and electric fields in the unit sphere (i.e., $R = B^{-1/4}$). The normalization is discussed in the Appendix. The $E0$ field is based on the difference in charge densities between the $S_{1/2}$ and $P_{3/2}$ orbitals.

Term	Trial	Exact	Error (%)
Fermions			
$\omega_{S_{1/2}}$	2.045	2.043	0.1
$\omega_{P_{3/2}}$	3.214	3.204	0.3
$S_{1/2}$-$S_{1/2}$ fields			
$M1$	-0.181α	-0.176α	3
$P_{3/2}$-$P_{3/2}$			
$M1$	-0.348α	-0.335α	4
$M3$	-0.068α	-0.067α	1
$E2$		0.108α	
$E0$		0.011α	
$\frac{1}{4}E2+E0$	0.040α	0.038α	5
$S_{1/2}$-$P_{3/2}$			
$E1$	0.218α	0.213α	2
$M2$	-0.094α	-0.093α	1

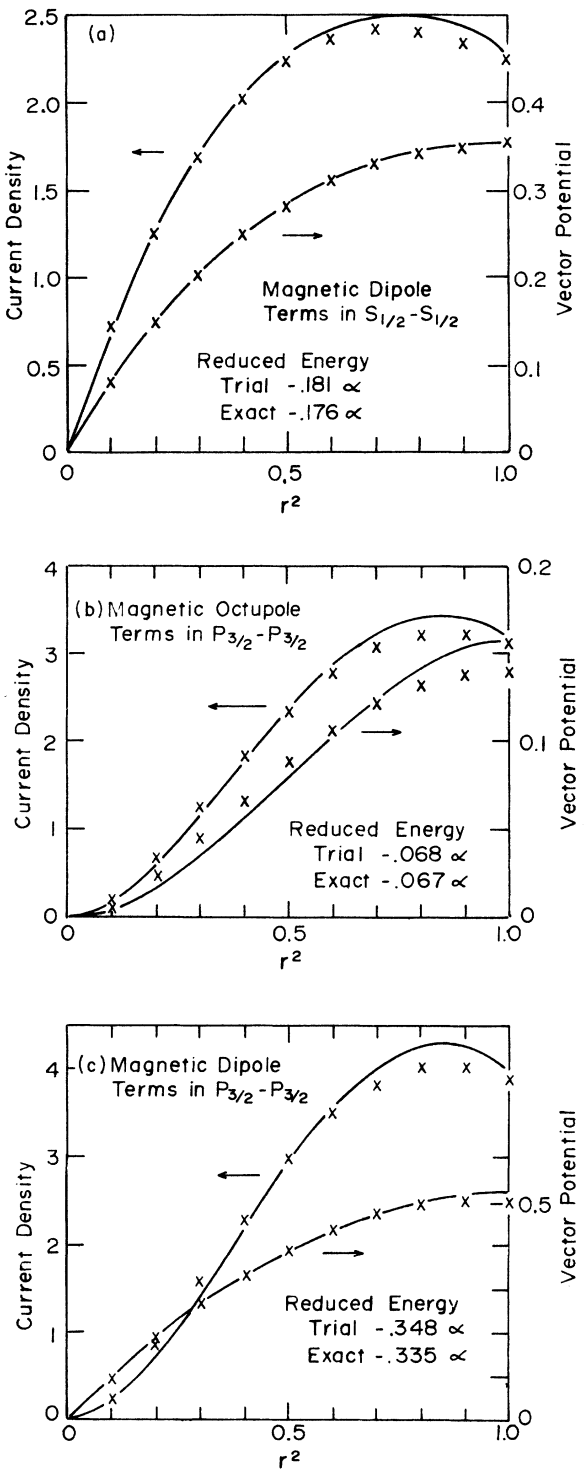

FIG. 5. Comparison of exact and best trial reduced current (left scale) and vector potential (right scale) coefficients for the unit sphere. The solid lines give the best trial value based on the trial fermion wave functions. The crosses show the exact values based on the exact currents. The normalization is described in the Appendix.

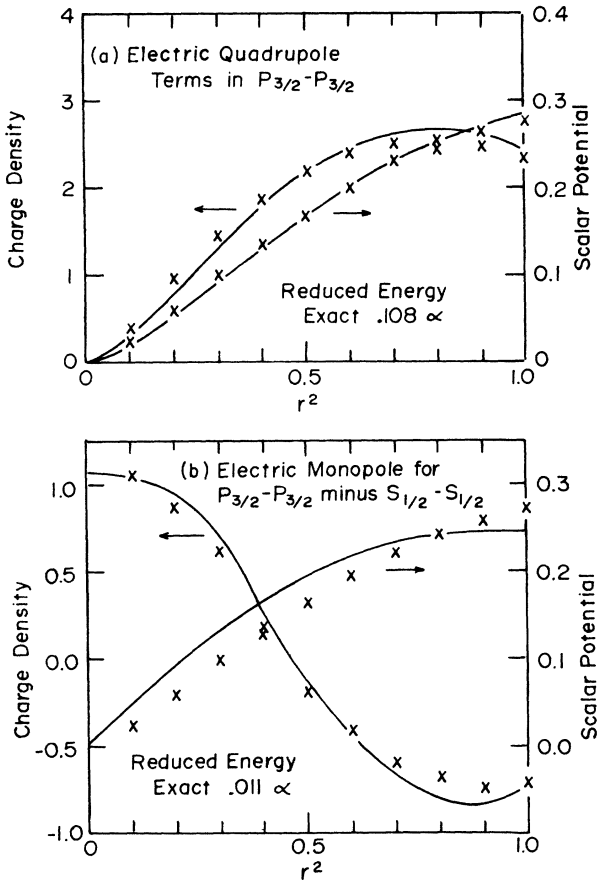

FIG. 6. Comparison of exact and best trial reduced charge density (left scale) and scalar potential (right scale) coefficients for the unit sphere. The crosses show the exact values; the solid lines, the trial values.

pole and quadrupole densities are obtained. (The static electric fields do not flip spins.)

The scalar potential difference is parameterized so that it imitates the form of ρ_D:

$$\phi_D = e_D z^2 + f_D , \tag{3.31}$$

where e_D and f_D are simple polynomials in R^2.

Computations for the unit sphere are compared in Fig. 6 with exact results based on the exact charge densities. The normalization of the "reduced coefficients" is analogous to that of the static color-magnetic fields (see the Appendix). The agreement is equally satisfactory.

3. *Time-dependent fields*

The expression

$$W_X = \int [\tfrac{1}{2}(|\vec{B}|^2 - |\vec{E}|^2) + \mathrm{Re}(\rho^*\phi - \vec{J}^* \cdot \vec{A})]\, dV , \tag{3.23}$$

with

$$\vec{E} = -\nabla\phi + i\omega A , \quad \vec{B} = \nabla \times \vec{A} , \quad \nabla \cdot \vec{J} = i\omega\rho \tag{3.33}$$

is stationary with respect to variations in ϕ and A when

$$\nabla \cdot \vec{E} = \rho , \quad \nabla \times \vec{B} = \vec{J} - i\omega\vec{E} \text{ in } V , \qquad \hat{n} \cdot \vec{E} = 0 , \quad \hat{n} \times \vec{B} = 0 \text{ on } S . \tag{3.34}$$

The stationary point is a maximum with respect to variations in ϕ and is a minimum with respect to variations in $\vec{A}$, provided that the lowest free-gluon frequencies are higher than ω, which is always the case in the present calculation. If the current is not exactly conserved, then the same problems with gauge dependence arise here as did in the static case, and they are dealt with in the same manner by fixing the gauge according to (3.17).

The variational expression (3.32) at the stationary point gives the contribution to the second-order energy shift due to an energy-conserving orbital transition $SA \to AS$. At the stationary point it has the value

$$W_X^0 = -\tfrac{1}{2}\,\mathrm{Re}\int (\rho^*\phi - \vec{J}^* \cdot \vec{A})\, dV . \tag{3.35}$$

For the diagrams of Fig. 3 we want to consider the off-diagonal transition $SS \to AA$. It was convenient in computation to evaluate these off-diagonal contributions to the energy by simply reversing one line of the energy-conserving diagram. Thus, after finding the stationary point of W_X, the resulting fields were then resubstituted into the expression

$$W_X' = -\tfrac{1}{2}\,\mathrm{Re}\int (\rho\phi - \vec{J} \cdot \vec{A})\, dV \tag{3.36}$$

to give the contribution which appears in (2.17).[13]

The transition current and charge densities based on (3.9) have the form

$$\begin{aligned} \rho_{SA} &= g(\phi_S\phi_A + s^2\chi_S\chi_A)(z - \kappa\sigma_z\sigma \cdot \vec{s}) , \\ \vec{J}_{SA} &= g\,[(\phi_S\phi_A - \chi_S\phi_A) iz\vec{s} + 2\kappa\chi_S\phi_A iz\vec{s}\sigma_z\sigma \cdot \vec{s} \\ &\quad - \kappa(\phi_S\chi_A + \chi_S\phi_A)s^2 iz\sigma_z\vec{\sigma} \\ &\quad + (\phi_S\chi_A + \chi_S\phi_A)z\sigma \times \vec{s}] . \end{aligned} \tag{3.37}$$

For the unit sphere, they produce electric dipole and magnetic quadrupole fields with both spin-flip and spin-nonflip transitions.

The trial scalar and vector potentials were selected to have the form

$$\begin{aligned} \vec{A}_{SA} &= h_x\,\sigma \cdot \vec{s}\hat{z} \times \vec{s} + d_x z\vec{\sigma} \times \vec{s} + ik_x(s^2\hat{z} - s_z\vec{s}) , \\ \phi_{SA} &= ib_x\vec{s} \cdot \hat{z} \times \sigma + j_x z + c_x z^3 . \end{aligned} \tag{3.38}$$

The choice was motivated by the form which yields

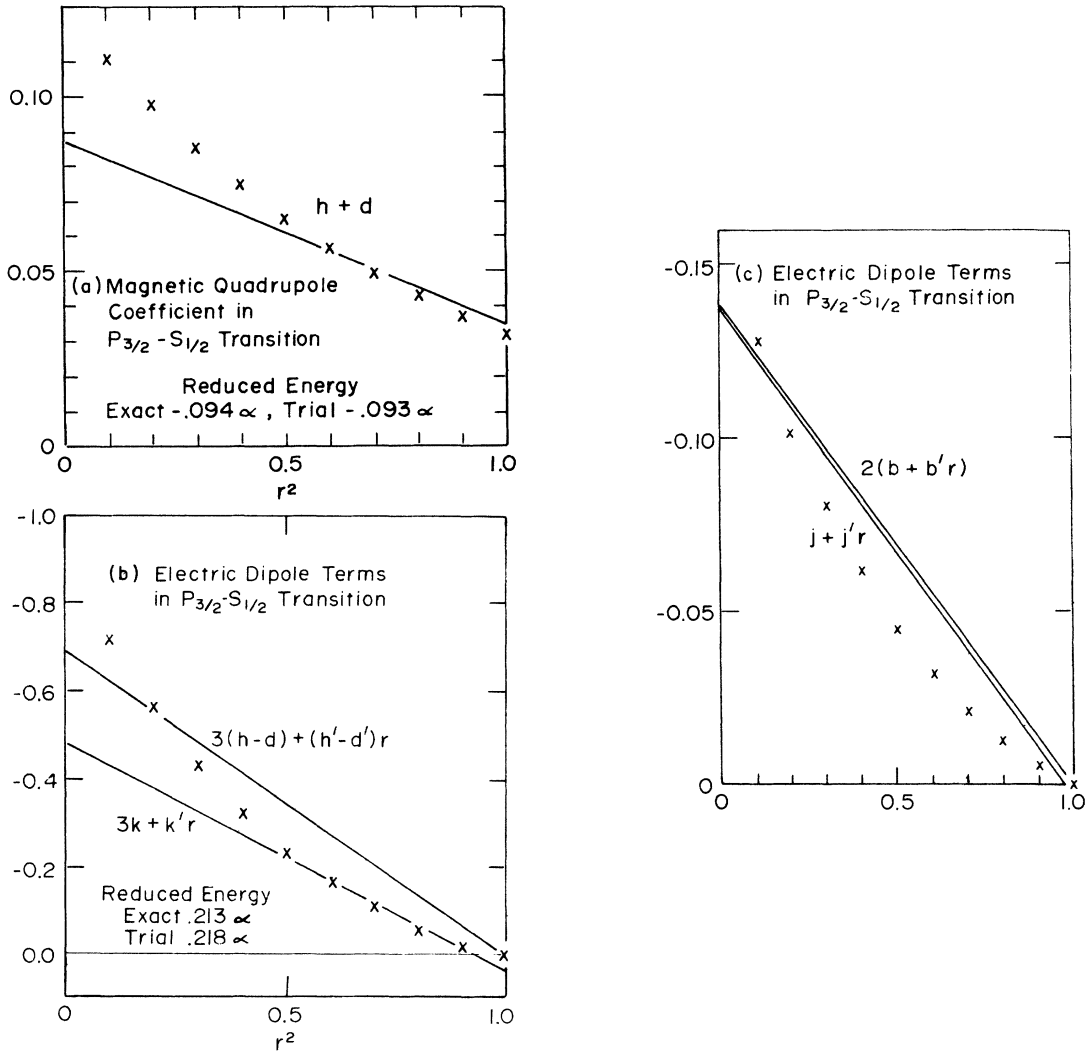

FIG. 7. Comparison of exact and trial expressions for the magnetic quadrupole and electric dipole coefficients for the $S_{1/2}$-$P_{3/2}$ transition in the sphere, as discussed in the Appendix. The crosses show the exact values. The solid lines show the trial values.

the exact solution for the sphere and by some experimentation. The coefficients h, d, k, b, and j are simple polynomials in R^2 and c is a constant. The last-mentioned electric octupole term was found to improve considerably the ability of the electric field to meet the linear boundary condition for nonspherical geometries.

As a test of the trail parameterization, the results of computations for the unit sphere are compared with the exact solution (also derived) in the Appendix and in Fig. 7. The agreement is quite satisfactory, and the error in determining the contribution to the energies is found to be a couple percent.

As a further check, the integrated electric flux across the equatorial plane was compared with an estimate of the integrated charge density for ellipsoidal shapes. It was found that to within the 15% accuracy of the method nearly all (i.e., 85% or more) of the flux remained confined to the hadron.

Of all the contributions to the energy from the transition fields, the most important is due to the spin-nonflip electric field characterized by the coefficients j_x and c_x in (3.38). Let us see what this term signifies. The transition charge density is constructed from a product of wave functions symmetric and antisymmetric under $z \to -z$. Thus as the cavity lengthens, the transition charge density describes the separation of opposite charges—basically positive for $z > 0$ and negative for $z < 0$. In the bag the associated color-electric flux lines are confined and so run along the de-

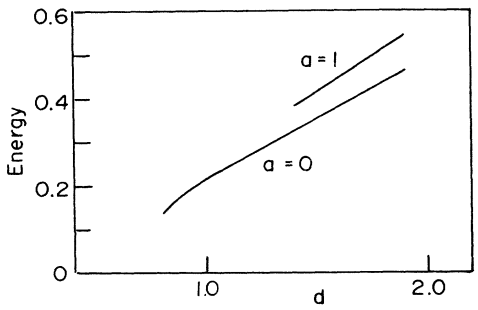

FIG. 8. Energy of the spin-independent transition field $(W_{EX}+W_{MX})/\alpha$ for two classes of cavity shapes plotted for increasing polar radius at fixed unit equatorial radius, as discussed in Sec. IIIC. Units are defined in terms of the bag constant B.

formation axis. This field is produced by terms with coefficients j_x and c_x in (3.38). As the cavity lengthens, the flux lines lengthen, and the contribution to the energy from the field grows. This effect is shown explicitly in Fig. 8, where the full spin-independent contribution (with the color fine-structure constant α removed) is plotted for cavities of ellipsoidal shape ($a=0$) and shapes defined by putting $a=1$ in (3.1), in both cases with unit equatorial radius, i.e., with surface defined by

$$\rho^2 = 1 - z^2/d^2 \text{ and } \rho^2 = 1 - z^4/d^2 . \tag{3.39}$$

The increase in energy is remarkably linear. For a discussion of the effect of this term upon the calculation, the reader is referred to Sec. IV.

D. Constraint

In the present calculation the constraint is imposed directly on the quark wave function. We suppose that left and right orbitals can be distinguished artifically by the operators z_R and z_L which have the property

$$\begin{aligned} z_R q_R(z_1)\bar{q}_L(z_2) &= z_1 q_R(z_1)\bar{q}_L(z_2) , \\ z_L q_R(z_1)\bar{q}_L(z_2) &= z_2 q_R(z_1)\bar{q}_L(z_2) . \end{aligned} \tag{3.40}$$

Then, using (2.2),

$$\delta = \langle z_R - z_L \rangle = \frac{2\sqrt{\mu}\,(1+\mu)}{1+\mu^2} \int q_S^\dagger(\vec{x}) q_A(\vec{x}) z \, dV . \tag{3.41}$$

Thus δ measures the average separation of left and right orbitals. It is naturally linear at small $\sqrt{\mu}$; and for two bags at large distance with $\mu=1$ it gives the classical separation distance.

The constraint is implemented by adding to the variational Hamiltonian the term

$$H \to H - c_\delta \delta . \tag{3.42}$$

At the expense of adding another orbital configuration, namely SA, the separation of a quark and antiquark into a spatially unsymmetrized wave function could be studied. In this case the constraint could take the form of an applied external (true Maxwellian) static electric field, instead of the rather artificial one used here. The intuitive pictures are identical, however, provided one imagines in the present calculation that half of the time the quark is on the right, and half on the time on the left. The conclusions should differ only in minor details. The spatially symmetric configuration is probably more appropriate to the study of rotationally induced deformations, and the spatially unsymmetrized configuration to the study of electromagnetic excitations.

The reader may be curious why we have not simply used the parameters defining the cavity geometry in order to impose the constraint, thereby sparing us the necessity of adjusting them against an internal constraint such as (3.42). In fact this procedure was attempted in the earliest stages of this study. With only the unperturbed fermion energies contributing to the energy, the length parameter d in (3.1) was fixed and a minimum was sought in the energy, varying the other two parameters. As soon as the length became substantial, the parameter a took on the value -1, corresponding to a cavity with nipples at the poles. This shape represents a tendency to reproduce the compact sphere that minimizes the energy in the absence of constraints as best as possible in keeping with the constraint. Had the parameterization allowed a wider range of shapes, the constraint would presumably have been satisfied by making a very thin projection from the poles of a sphere. It became clear that a sensible calculation was needed to make the surface respond to the constrained fields rather than vice versa.

E. Zero-point energy

We do not attempt to find the zero-point energy of the fermion and gluon fields as a function of cavity shape. Our only knowledge of this term comes from calculations of the masses of the light hadrons where including it is important. We have made a plausible guess about its shape dependence based on the following argument: The zero-point energy should scale linearly with the energy eigenvalues, and should double in value if the energy levels become pairwise degenerate. We have at our disposal only two energies—those of the two lowest fermion orbitals ω_S and ω_A. If the value of the zero-point energy is Z_0^S/R for the sphere of radius R, then it becomes $2Z_0^S/R$, should the sphere divide into two spheres of the same radius. In the same limit ω_S and ω_A are degenerate with the single sphere energy. Thus

$$E_0 = -Z_0^S\left(\frac{2\omega_S}{2.043} - \frac{\omega_A - \omega_S}{1.161}\right) \tag{3.43}$$

is a simple choice with all of the desired properties. (For the sphere $\omega_S = 2.043/R$, $\omega_A - \omega_S = 1.161/R$.) For ellipsoidal cavities of unit equatorial radius, E_0 increases by 10% when the major axis is doubled in length. Thus our guess has negligible effect upon the present quark-antiquark calculation, but it becomes important when the cavity undergoes fission.

F. Quark self-energy

These contributions are represented by the diagrams Figs. 3(b) and 3(f) in our two-orbital approach. In the calculation of the masses of the light hadrons of Ref. 2 only one orbital was considered and only the electric part of the diagonal S-S-S term was included, since it was required in order to satisfy the linear boundary condition for the electric field. For various reasons we cannot ignore the off-diagonal S-A-S and A-S-A contributions. For one reason, if we follow the approach of Ref. 2 strictly and use their parameters, the ρ meson is not stable (see Sec. IV) in the static cavity approximation. Although this result might be dismissed as a defect of the whole approach, there is another reason. We expect that when the quark and antiquark are widely separated, the field energy should correspond to the energy of two opposite classical charges. A careful examination of the normalizations of the various terms shows that the term W_{EX} gives the electrostatic energy of the separation of two color charges of *half* strength. Thus, to get the energy of separation of two opposite color charges of full strength, the term should be multiplied by a factor of four when $\mu \to 1$. A factor of two comes from the diagram in which a gluon is exchanged. The other term with a factor of two comes from the self-energy. To see this result, note that in (2.17) W_{EX} is multiplied by $(C_X + n_S^c + n_A^c)$, which, from (2.21), is $(4\mu/N + 2)\frac{16}{3}$; also note that $N \to 2$ when $\mu \to 1$.

Therefore, if we are to make contact on the one hand with Ref. 2 when the quark and antiquark are unseparated and on the other hand with our classical expectations when they are widely separated, the off-diagonal self-energy terms must somehow be canceled for a nearly spherical configuration and grow in importance for long bags. Since the full self-energy contribution involving a summation over all intermediate states has not been performed, it must be estimated. The details of the estimate are presented in the following paper[7] because its effects upon the two-nucleon interaction are more profound. The estimate obtained in Ref. 7 is based on the observation that for the sphere the negative magnetic terms represented in (2.17b) by $W_{MS\parallel}$, $W_{MS\perp}$, $W_{MA\parallel}$, and $W_{MA\perp}$ nearly cancel the full electric dipole contribution represented by W_{EX}. [The other terms in (2.17b) are small and are dropped.] As the cavity lengthens, the magnetic terms fall off and the electric term grows. Thus there is a natural tendency in these terms to recover the result described above. (Of course contributions from higher orbitals not considered here may alter the result.)

The self-energy is written as

$$E_{\text{self}} = n_S \delta\omega_S + n_A \delta\omega_A , \tag{3.44}$$

in terms of the self-energies of the separate orbitals. The approximation takes the explicit form

$$\delta\omega_S = \tfrac{16}{3}\left[W_{EX} + W_{MX} + c_1 n/d^2 R_0 + (W_{MS\parallel} + 2W_{MS\perp})xc_2\right]$$

$$\delta\omega_A = \tfrac{16}{3}\left[W_{EX} + W_{MX} + (W_{MA\parallel} + 2W_{MA\perp})xc_3\right] \tag{3.45}$$

$$x \equiv 1 - (1 - n/d)^2 , \quad c_1 = 0.081 , \quad c_2 = 1.34 , \quad c_3 = 0.93$$

G. Computational procedure

The order of computation is as follows:

(i) Choose a cavity shape.

(ii) Find the best trial fermion orbital wave functions and energies in the absence of gluon couplings.

(iii) Construct the two diagonal and one off-diagonal four-current densities from the wave functions.

(iv) Find the best trial expressions for the color-electric and -magnetic fields based on the current densities so obtained. Construct from the fields the configuration-independent coefficients $W_{MS\perp}$, etc., appearing in (2.17).

(v) Evaluate the configuration-dependent energy and constraint terms (2.17) and (3.41) and find the minimum as a function of μ for a given value of the Lagrange multiplier c_δ.

Steps (i)–(v) are repeated as the shape is varied and the overall minimum is sought for each value of c_δ. This leads to the determination of the energy as a function of the "expectation value" of the separation parameter.

The procedure outlined above gives a particular order of computation. Others may be contemplated. Let us consider its effect in aggregate upon the results. Because the component fermion orbitals are constructed independently of the gluon fields, distortions of these orbitals due to the presence of the fields is not taken into account. However the gross modification of the orbitals due to the gluon couplings and the constraint is taken into account in the sense that new orbitals called

"left" and "right" emerge as a result of configuration mixing. Because the constraint enters the computation in step (v) only after the field energies are obtained, its effect upon, for example, the component fermion wave functions is not taken into account. However, its important effect upon the left-right separation is, of course, taken into account. None of these secondary effects were judged to be of any consequence. However, if one wanted to take them into account, one could combine steps (ii)–(v) into one grand variational scheme in which all parameters are varied simultaneously. The advantage of the approach we have adopted is that it makes each step clearcut and more readily checked computationally (as we have done in the Appendix), and it requires less computer time. Related to the latter advantage is the useful feature that the contributions to the field energies obtained in steps (ii) and (iii) are configuration and constraint independent. They depend only on the cavity shape. Thus once they have been computed, they may be substituted into algebraic expressions of the type (2.17) for any desired color-singlet configuration involving the two orbitals without the need to repeat the time-consuming steps (ii)–(iii).

Calculations were carried out with a high-speed digital computer. Integrations over the cylindrical coordinate ρ were carried out exactly, in some instances making use of Gaussian quadrature, and over the coordinate z, numerically, using an eight-point Gaussian quadrature. A total of four parameters (and two normalization constants and the configuration-mixing parameter μ) for the fermion wave function and the twelve parameters (and four normalization constants) for the gluon vector potentials were adjusted.

Rather than having the computer automatically adjust shapes for the minimum energy, this was done by hand. This procedure was more effective since the energy was rather insensitive to some of the geometrical parameters, enough so that minor fluctuations in the energy due to the adjustment of field parameters prevented a precise determination of the shape. The procedure adopted was to take advantage of the dimensional scaling properties of the field energies, constraint, and volume term for zero-mass fields. The computation was carried out at a fixed cavity proportion n/d and fixed a [see (3.1)], the overall scale being found by solving the quartic equation

$$\frac{d}{d\xi}\left(E^0_{\text{field}}/\xi + E^0_{\text{vol}}\,\xi^3 - c_\delta\,\delta^0\xi\right) = 0\,, \tag{3.46}$$

where the quantities with superscript 0 are the scale-independent energies for the total field energy, bag volume energy, and separation, respectively. It was a simple matter to display the results for various choices of the Lagrange multiplier c_δ and the parameters n/d and a, and select the overall minimum for each c_δ. Because of the relative insensitivity of the calculation to the choice of n/d and a, it was not necessary to consider more than about fifty pairs of values. In some cases the variation in the minimum value for different selected cavity proportions was less than the error in the minimum value itself. An unambiguous result was obtained by drawing curves of E_{tot} vs δ for each of the various cavity proportions in question. The envelope of the curves was clearly defined, and points lying closest to the envelope were chosen.

IV. RESULTS AND CONCLUSIONS

We present and discuss the results of computations for a state with quantum numbers of the ρ meson (2.12) with spin projection $|m_S| = 1$ on the deformation axis. We use throughout essentially the parameters of Ref. 2 for massless quarks, namely $\alpha_c = 0.54$, $B^{1/4} = 145$ MeV, and E_0 for the sphere given by (3.43).

A. Ground states without constraint

If all self-energy contributions (3.45) are omitted except for those required to satisfy the boundary condition for the electric field, as in Ref. 2, the ρ meson (2.12) is found to be unstable even without the production of an additional quark-antiquark pair. The energy of the cavity is lowered by an elongation of the bag relative to the equatorial radius with both the quark and the antiquark kept in the symmetric orbital (i.e, $\mu = 0$ always). This effect persists while a neck is formed and, although it was not actually followed to its conclusion, it presumably ends with the fissioning of the bag into two peculiar bags of mass ~200 MeV, each containing a quark and an antiquark with the wrong normalization for a single cavity, namely with

$$\int q_S^\dagger q_S\, dV = \tfrac{1}{2}\,. \tag{4.1}$$

Unit normalization is obtained only when both cavities are included in V.

The origin of this instability may be sought by examining the behavior of the fermion kinetic energy ω_S as the bag lengthens at a fixed equatorial radius. It decreases (see Fig. 2). So does the energy of the magnetic field, $W_{MS\parallel}$, $W_{MS\perp}$. When the negative zero-point energy E_0 (3.43) is included, the result is a term which falls quite rapidly. Thus the cavity may shrink so as to actually reduce the total volume as the ratio of polar to equatorial radius grows. When the cavity shrinks, the field energy is increased again, but

not enough to compensate for the loss of volume energy. The actual amount by which the energy is reduced depends sensitively on the handling of the zero-point energy E_0. Consider the energy at the onset of neck formation when $d/n = 1.5$ and $a = 1$ in (3.1). With the expression (3.43) the energy of the "ρ meson" has fallen to 680 MeV. If we set instead $E_0 = -Z_0^s/n$, the energy is reduced to 740 MeV.

Nothing within the confines of the static cavity treatment prevents such a configuration from appearing, since the quantization condition of unit normalization is only semiclassical. The only fully quantized bag theory presently available is restricted to one spatial dimension.[1] In this theory, only two boundary points are ever associated with a single quantum, not four as in two bags. Thus we may regard this instability as indicating a breakdown of the static cavity approximation; perhaps it is a reflection of the normal decay into lighter mesons in a properly quantized theory.

Since we believe the self-energy term (3.45) should be included, we find that the ρ meson is stable with respect to small deformations from a roughly spherical shape. In effect the self-energy term introduces a barrier against the collapse discussed above. Nevertheless, deformations from a spherical shape do not cost much in energy. For example, if we restrict our attention to ellipsoidal shapes, even with the spherical stability provided by the self-energy, a variation of ±10% in the ratio of polar to equatorial radius from the sphere produces a variation of 2–3% in the energy of the state. When the parameter a is permitted to vary, the energy is reduced by 3% at the minimum, which occurs at $a = -0.5$. This effect is very likely an artifact of the self-energy approximation (3.45) since it is associated with a decrease in the value of E_{self}. In any event we do not claim accuracy to this level; so we prefer to fix $a \geq 0$, thereby starting the calculation off with a spherical shape at the lowest energy—namely, 780 MeV with a cavity radius of 0.932 fm.

B. Deformed states with constraint

In Fig. 9 the main result of the computation is shown. The bag energy is seen to rise rapidly as a function of the separation parameter. In Fig. 10 we present the shapes of the cavity at the points with the corresponding labels A, B, and C in Fig. 9. The equatorial radius is seen to approach a constant value quite rapidly. The parameter a in (3.1) takes on the value 1 at $\delta \approx 1.75$ fm. This is the value which makes the cavity most like a cylinder in the middle, since the surface then is given by

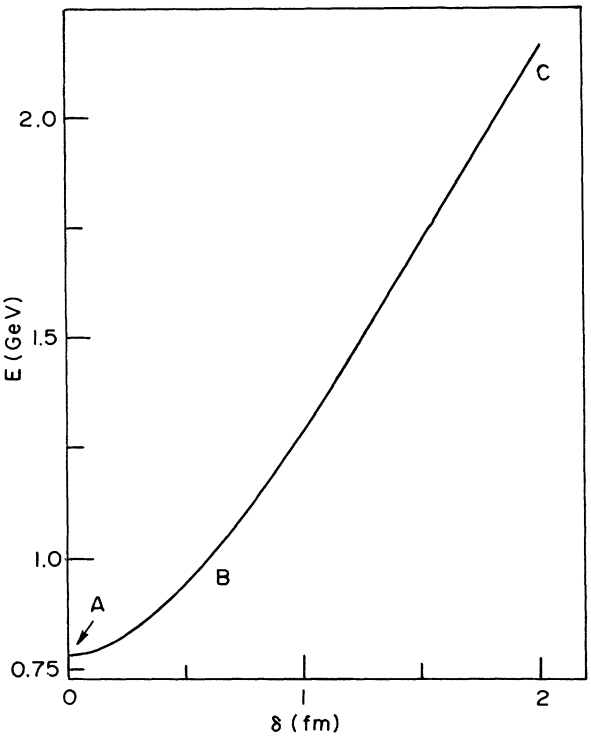

FIG. 9. Energy of the deformed cavity state (GeV) as a function of the measure of quark separation (fm).

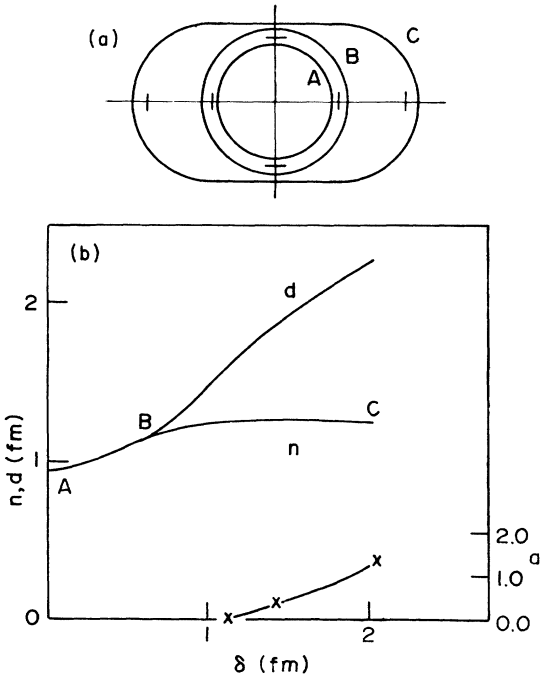

FIG. 10. (a) Shapes of the cavity at selected points A, B, and C in Fig. 9. Scale markings are in fermis. (b) Parameters defining cavity shape [cf. (3.1)] as a function of separation.

$$\rho^2 = n^2(1 - z^4/d^4) . \tag{4.2}$$

Values of $a \gg 1$ correspond to the onset of the formation of a neck. These values were never preferred in the variational calculation, which confirms the expectation that the bag will not undergo fission into two bags of one quark and antiquark—this fission being prevented by the pressure exerted by the color electric field linking the quark and antiquark. Calculations (not shown) at large values of a give extremely large values for the color-electrostatic energy W_{EX}.

Let us see whether we can account for the slope and cylindrical radius of the long bag with a crude model which takes into account the color-electrostatic field produced by the color separation. Imagine the electrostatics problem of a cylindrical cavity of length $2l$ and cross-sectional area A, filled uniformly with a charge of $-q$ for $z > 0$ and uniformly with a charge of $+q$ for $z < 0$. With the surface boundary condition $\hat{n} \cdot \vec{E} = 0$, the field has the form

$$\vec{E} = \frac{q}{A} (1 - |z/l|)\hat{z} , \tag{4.3}$$

and the total electrostatic energy is

$$W_{EX} = \tfrac{1}{2} \int \vec{E}^2 dV = \frac{1}{3} \frac{q^2}{A} l . \tag{4.4}$$

In the present calculation what should we take for q^2? If the symmetric and antisymmetric wave functions were identical except for the sign in each half of the cavity, as they would be if the cavity were fissioning, the total charge in half of the cavity ($z < 0$) would be $g\lambda^a$. Actually it is less than this because the wave functions do differ in magnitude for nonfissioning shapes. Using our crude model for the cavity and computing the separation parameter (3.41) for $\mu = 1$ and comparing the result with computed results, we obtain the estimate $\delta = 0.8l$ and a charge of $0.8 \times g\lambda^a$ for half of the bag, for the shapes relevant to the present discussion. Therefore

$$q^2 \approx 0.64 g^2 (\tfrac{16}{3}) . \tag{4.5}$$

If the color-electric energy gives the most important contribution to the field pressure along the sides near the equator, then the cavity radius at equilibrium can be found from minimizing the energy

$$E(l) = BAl + \tfrac{1}{3} q^2 l / A , \tag{4.6}$$

with respect to variations in A. Hence

$$A = \pi\rho^2 = \left(\frac{q^2}{3B}\right)^{1/2} , \quad \rho \approx 0.94 B^{-1/4} , \tag{4.7}$$

to be compared with the calculated value of $0.91B^{-1/4}$. The slope of the curve of energy vs separation may be found by substituting (4.7) into (4.6) and dividing by the estimate for δ given above (4.5). The result is independent of the factor 0.8 used to correct the charge normalization and is

$$E/\delta \approx 7B^{1/2} , \tag{4.8}$$

to be compared with $8.6B^{1/2}$ found at the greatest values of δ in Fig. 9. Considering the approximate nature of the estimate (4.8) we can say that our qualitative expectations are confirmed.

Returning to the computed results, let us consider the various contributions to the total energy displayed in Figs. 11 and 12 and Table III as a function of quark separation. The combined field energy (excluding the zero-point energy) and bag volume energies both rise rapidly as shown in Fig. 11. The presence of a substantial fermion component is indicated at the greatest separation considered here, since in our crude asymptotic model above, we would expect that the field and volume energies would approach each other asymptotically. Our suspicion is confirmed in Fig. 12 where it is seen that the rapidly rising gluon terms labeled (c) and (d) have not yet overwhelmed the slowly falling fermion energy (a) at large separations. The contribution labeled (d) is the self-energy. It is nearly equal to the large off-diagonal gluon-exchange term (c); and it is negligible at small

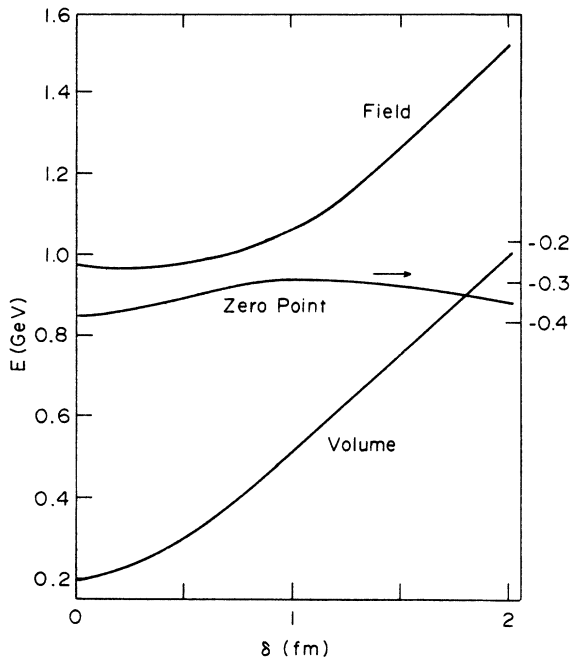

FIG. 11. Contribution to the cavity energy from total field energy, volume energy, and zero-point energy (scale on right) as a function of the quark separation.

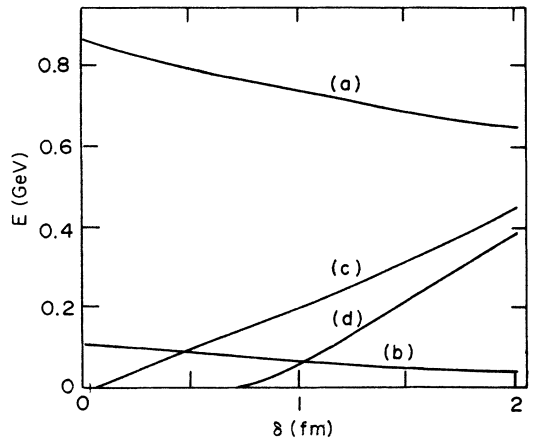

FIG. 12. Contribution to the field energy from (a) fermion kinetic energy, (b) diagonal gluon exchange, (c) off-diagonal gluon exchange, and (d) self-energy as a function of separation.

separations, because these separations occur for nearly spherical shapes. Both of these criteria were specified in the discussion of Sec. III F. The diagonal gluon exchange is purely magnetic and its energy contribution (b) decreases slowly at large separation. The configuration-mixing parameter plotted in Fig. 13 rises rapidly to $\mu \approx 1$ corresponding to nearly orthogonal left and right orbitals.

C. Conclusions

Aside from errors associated with the choice of the model—i.e., the static cavity approximation, the neglect of states with extra gluons, the truncation of the perturbation series at second order in gluon exchange, etc.—there are a variety of other sources of possible error. Probably the most important of these is in the approximation used to calculate the self-energy. Although the criteria discussed in Sec. III F above and in Ref. 7 impose bounds on the form of (3.45) there is still considerable latitude allowed. It is not inconceivable that for the configuration (2.12) considered here, the self-energy term was in error by 30%, thereby introducing a 10% error in the total energy at the largest separations. This error does not affect the calculation for small separations in the same way, since we are then in the nearly spherical regime where the phenomenological values of the constants of Ref. 2 apply. Of the errors associated with the variational calculation itself, the least serious comes from the determination of the fermion kinetic energy, which is probably good to 1% over the range of shapes in question. As for the gluon contribution, from our comparison with exact calculations in the sphere and from experimentation with the trial parametrization, it is estimated that errors of 10% in the determination of these energies might be expected at large separations, i.e., an error comparable to that estimated to be introduced by the approximation of using degenerate second-order perturbation theory for the gluon contribution, leading to an error of about 5% in the total energy at large separation.

Although it may be of some use to learn that it costs about 250 MeV to separate a quark from an antiquark by a distance of $\frac{1}{2}$ fm when their spins are parallel along the line of separation, the methods we have developed could have a much wider

TABLE III. Energy contributions, geometrical and configuration parameters for the ρ-meson–like bag with spin projection 1 on the deformation axis at various separations (δ) of the quark and antiquark. All energies are given in MeV, lengths are given in fm. $E_{\rm tot}$ is the total energy; $E_{\rm F}$ is the total fermion energy; $E_{\rm diag}$ is the contribution from orbital-preserving gluon exchange; $E_{\rm trans}$ is the contribution from orbital-changing gluon exchange; $E_{\rm self}$ is the self-energy contribution; E_0 is the zero-point energy; and $E_{\rm vol}$ is the bag volume energy. The geometrical and configuration parameters are defined in Sec. III A.

δ	μ	$E_{\rm tot}$	$E_{\rm F}$	$E_{\rm diag}$	$E_{\rm trans}$	$E_{\rm self}$	E_0	$E_{\rm vol}$	d	n	a
0.00	0.000	779	866	111	0	−2	−389	193	0.93	0.93	0.0
0.05	0.008	783	862	110	3	−2	−388	198	0.94	0.94	0.0
0.12	0.032	794	852	109	13	−2	−383	205	0.95	0.95	0.0
0.22	0.085	818	834	106	33	−2	−374	221	0.97	0.97	0.0
0.34	0.180	867	808	100	65	−2	−357	253	1.02	1.02	0.0
0.52	0.331	952	787	91	104	−2	−335	306	1.08	1.08	0.0
0.65	0.478	1035	778	82	128	−2	−317	364	1.15	1.15	0.0
0.86	0.629	1171	758	72	170	24	−306	452	1.31	1.19	0.0
1.13	0.747	1388	721	61	228	94	−304	587	1.61	1.23	0.0
1.47	0.836	1692	684	55	308	210	−318	751	1.86	1.24	0.4
2.00	0.915	2169	641	45	445	384	−348	1000	2.22	1.24	1.2

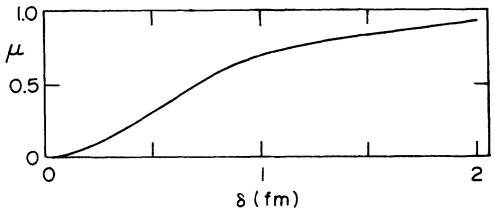

FIG. 13. Configuration-mixing parameter μ as a function of separation.

application in the study of rotational excitations of the mesons. Theoretical studies in the bag model to date[6] have obtained quite reasonable values for the slopes of various Regge trajectories, assuming the rotationally excited state takes on the form of a long, rotationg cylinder with the quarks at the ends. It would be of considerable interest to carry out a calculation of the type presented here using as a constraint, instead of the quark separation, the term

$$\omega_y J_y \ , \tag{4.9}$$

where $\vec{J}$ is the total angular momentum of the fields. It is not immediately obvious that axially elongated shapes would necessarily occur for small rotational velocities ω_y. Nor is it obvious in what way, if at all, the quarks would be thrown out toward the ends at larger ω_y.

The calculation presented here represents the first effort at treating the deformation properties of bags containing massless quarks. Many things have of necessity been omitted from the calculation in the interest of simplicity, including the full self-energy of the fields, the center-of-mass motion, surface fluctuations, the projection onto states of definite total angular momentum, terms of higher order in the gluon coupling, states containing gluons and extra quark-antiquark pairs. With time these improvements may be incorporated. That the results correspond favorably to naive theoretical expectations supports our optimism that the computational techniques presented here are sound and may be applied with some confidence to the more difficult problems of resonance decay and the two-nucleon interaction.

ACKNOWLEDGMENTS

This work was begun in collaboration with several members of the Center of Theoretical Physics, each of whom contributed significantly to its early theoretical development—in particular Alan Chodos, Barry Freedman, Kenneth Johnson, Jospeph Kiskis, Ernest Moniz, and Charles Thorn. Special thanks are also due to Arthur Kerman and John Negele for discussions of related calculations in nuclear physics. It should be mentioned that Alan Chodos and Ernest Moniz are currently pursuing an alternative formulation of the bag deformation problem and we have benefited mutually by comparing observations on nearly all details of the calculation.

APPENDIX: COMPARISON WITH EXACT CALCULATION FOR THE SPHERE

The unperturbed quark wave functions for the sphere are well known[1,2] and are compared in Sec. III B and Fig. 4 with our best trial wave functions. From the trial wave functions (3.9) the trial currents for the transitions S-S, A-A, and A-S are constructed and the gluon fields are computed variationally as discussed in Sec. III C. The resulting field components and energies may be compared in the sphere with the equivalent components and energies calculated from the exact wave functions. We take the gluon fields in order.

A. Static color-magnetic and -electric fields

The exact expression for the magnetic field for the diagonal S-S transition has been given in Ref. 2. We have repeated the calculation and also obtained the exact field components for the A-A transition by a direct numerical integration of the field equations.

In the unit sphere the vector potentials $\vec{A}_{SS}$ and $\vec{A}_{AA}$ (both exact and trial) can be written in such a way that the magnetic dipole and octupole terms are evident,

$$\begin{aligned} \vec{A}_{SS} &= \vec{r} \times \nabla[a_{1S}(\sigma \cdot \vec{r})] \ , \\ \vec{A}_{AA} &= \vec{r} \times \nabla[a_{1A}(\sigma_z z - 2\sigma \cdot \vec{r}) \\ &\quad + a_{3A}(\sigma \cdot \vec{r} z^2 - \tfrac{2}{5} z \sigma_z r^2 - \tfrac{1}{5} \sigma \cdot \vec{r} r^2)] \ . \end{aligned} \tag{A1}$$

In this special case the coefficient functions in (3.26) are

$$\begin{aligned} b_A &= -2d_A = 2a_{3A} \\ a_A &= 2a_{1A} + \tfrac{1}{5} a_{3A} r^2 \\ c_A &= -a_{1A} + \tfrac{2}{5} a_{3A} r^2 \ . \end{aligned} \tag{A2}$$

Exact and trial values for the magnetic dipole (a_{1S}, a_{1A}) and octupole (a_{3A}) coefficients are compared in Fig. 5. The coefficient functions shown have been normalized so as to emphasize the way in which they contribute to the energy in the following manner: In a spherical geometry the contributions of the multipole fields to the spin-flip and spin-nonflip terms in the energy are related by Clebsch-Gordan coefficients. We define a set of "reduced energies" $\bar{U}_{1S}$, $\bar{U}_{1A}$, and $\bar{U}_{3A}$ in which these spin-dependent factors are removed. In addition the color-dependent factor $\lambda_1^a \cdot \lambda_2^a$ is removed. Thus for example the spin-flip transi-

tion within the $P_{3/2}$ level mediated by the octupole field contributes, in the notation of (2.17),

$$W_{MA1} = \left| \langle \tfrac{3}{2}\tfrac{1}{2}, \tfrac{3}{2}\tfrac{1}{2} \mid 31 \rangle \right|^2 \bar{U}_{3A} . \tag{A3}$$

The other contributions may be obtained in a similar fashion. The reduced energies for the various multipole terms may be obtained by integrating the product of a current coefficient in (3.24) with the corresponding vector potential coefficient in (A1) multiplied by a kernel of the form cr^n. The square root of this kernel is assigned to each coefficient, thereby defining the reduced current and multipole coefficients, so that

$$\bar{U}_{1S} = -\frac{\alpha}{2}\int \bar{a}_{1S}\bar{j}_{1S}\,dr , \quad \bar{U}_{1A} = -\frac{\alpha}{2}\int \bar{a}_{1A}\bar{j}_{1A}\,dr ,$$
$$\bar{U}_{3A} = -\frac{\alpha}{2}\int \bar{a}_{3A}\bar{j}_{3A}\,dr . \tag{A4}$$

These are the coefficients plotted in Fig. 5. The agreement is quite satisfactory, considering that only three parameters and three normalization factors were used. The errors in the calculated reduced energies are a few percent or less and are summarized in Table II.

The comparison in Fig. 6 and Table II of the electric monopole and quadrupole terms in the static color electric field (3.31) follows the same normalization procedure.

B. The transition fields

Rather than carrying out a direct integration of the field equations to produce these terms, we used an expansion in terms of vector spherical harmonics.[14] The exact solution for the sphere has the form

$$\vec{B}_{SA} = \sum_n \eta_1^n j_1(\omega_{1n}r)\vec{X}_1 - \frac{i}{\omega}\sum_n \beta_2^n \nabla\times j_2(\omega_{2n}r)\vec{X}_2 ,$$
$$\vec{E}_{SA} = \frac{i}{\omega}\sum_n \eta_1^n \nabla\times j_1(\omega_{1n}r)\vec{X}_1 + \sum_n \frac{\omega_{2n}^2}{\omega^2}\beta_2^n j_2(\omega_{2n}r)\vec{X}_2 - \frac{i}{\omega}\vec{J}_{SA} , \tag{A5}$$

where

$$\vec{X}_1 = \tfrac{1}{2}\vec{L}(z/r - \tfrac{1}{2}\vec{r}\cdot\hat{z}\times\sigma/r)$$
$$\vec{X}_2 = \tfrac{1}{6}\vec{L}(3\sigma\cdot\hat{r}z/r - \sigma_z) \tag{A6}$$
$$j_1(\omega_{1n}) = 0 , \quad \frac{d}{dr}[rj_2(\omega_{2n}r)]\Big|_{r=1} = 0 , \quad \vec{L} = \frac{1}{i}\vec{r}\times\nabla .$$

The electric dipole and magnetic quadrupole coefficients η_1^n and β_2^n are projected from the current and charge densities (3.37) through

$$\eta_1^n = \frac{2\omega}{3}\frac{1}{N_{1n}^2(\omega^2-\omega_{1n}^2)} \times \int_0^1 r^2dr\left\{(\phi_S\phi_A + \chi_S\chi_A r^2)\frac{d}{dr}[rj_1(\omega_{1n}r)] - \frac{\omega_{1n}^2}{\omega}r(\phi_S\chi_A - \chi_S\phi_A)j_1(\omega_{1n}r)\right\} ,$$

$$\beta_2^n = -\omega\frac{1}{N_{2n}^2(\omega^2-\omega_{2n}^2)}\int_0^1 r^2dr(\phi_S\chi_A + \chi_S\phi_A)j_2(\omega_{2n}r) ,$$

$$N_{1n}^2 \equiv \int_0^1 r^2dr[j_1(\omega_{1n}r)]^2 . \tag{A7}$$

Contact with the notation of (3.38) is made through the following expressions which hold for the sphere:

$$h + d = \frac{1}{\omega r^2}\sum_n \beta_2^n j_2(\omega_{2n}r) ,$$
$$3k + k'r = -\frac{1}{r}\sum_n \eta_1^n j_1(\omega_{1n}r) , \tag{A8a}$$
$$k = h - d ,$$
$$\omega(j + j'r) - 2(3k + k'r) = \tfrac{2}{3}(\phi_S\chi_A - \chi_S\phi_A)r^2 ;$$
$$j = 2b , \tag{A8b}$$
$$c = 0 .$$

Thus all quantitites are determined from the two series in the expressions (A8a) above. The exact fields were obtained by carrying out the projection (A7) numerically for the lowest four radial modes, using the exact expressions (3.13) for the fermion wave functions. The series (A8a) converged very rapidly and gave the values plotted with crosses in Fig. 7. These are compared with trial values for $h + d$, $3k + k'r$, and $3(h - d) + (h - d)'r$. The centrifugal barrier factors have not been included in the coefficients plotted here, as they were in the previous figures. Thus the disagreement is not as serious as it would appear for small r^2. The reduced energies, defined by dividing out the appropriate Clebsch-Gordan coefficients as before agree with the variationally determined values to within a couple percent as indicated in Table II.

*This work is supported in part through funds provided by ERDA under Contract No. EY-76-C-02-3069.
†Work supported in part by the A. P. Sloan Foundation.

[1]A. Chodos, R. L. Jaffe, K. Johnson, C. B. Thorn, and V. F. Weisskopf, Phys. Rev. D 9, 3471 (1974); A. Chodos, R. L. Jaffe, K. Johnson, and C. B. Thorn, *ibid.* 10, 2599 (1974).
[2]T. DeGrand, R. L. Jaffe, K. Johnson, and J. Kiskis,

Phys. Rev. D 12, 2060 (1975).
[3]P. N. Bogoliubov, Ann. Inst. Henri Poincafe 8, 163 (1967).
[4]C. Rebbi, Phys. Rev. D 12, 2407 (1975).
[5]P. Hasenfratz, J. Kuti, and A. Szalay, in *Charm, Color and the J/ψ*, proceedings of X Rencontre de Moriond, Méribel-les-Allues, France, 1975, edited by J. Trân Thanh Vân (CNRS, Paris, 1975).
[6]K. Johnson and C. B. Thorn, Phys. Rev. D 13, 1934 (1976).
[7]C. DeTar, following paper, Phys. Rev. D 17, 323 (1978).
[8]The converse is not true. Satisfying the nonlinear boundary condition does not always guarantee a minimum energy. See Sec. IV A.
[9]A. Chodos, private communication, 1976.
[10]The advantages of appealing to degenerate perturbation theory and the approximations leading to a calculation with static fields have been stressed by A. Chodos and E. Moniz (private communication).
[11]Actually, no solution for $\vec{E}_{SS}$ exists since the boundary condition (1.8) cannot be met for a nonvanishing total charge. However, since the state is a color singlet, these fields do not contribute to the total energy, as may be seen in (2.20); so we are spared from calculating them. The purpose of their appearance here is merely didactic.
[12]This method of obtaining the fermion eigenvalues is due to C. Thorn (private communication).
[13]The relative phase of the wave functions (3.9) is fixed to be real by the physical criterion that the orbitals (2.2) define a left-right separation with positive μ, and by the approximation of degeneracy. Thus there is no ambiguity in reversing the line of the graph. Any difference between (3.35) and (3.36) is, in fact, of the order $(\omega_S - \omega_A)^2/\omega_G{}^2$ and could as well have been ignored in the spirit of the approximation discussed at the beginning of Sec. III C.
[14]See, for example, J. D. Jackson, *Classical Electrodynamics* (Wiley, New York, 1975).